2015-12-01

Intraflagellar transport is essential for mammalian spermiogenesis but is absent in mature sperm

Jovenal T. San Agustin
University of Massachusetts Medical School

Et al.

Intraflagellar transport is essential for mammalian spermiogenesis but is absent in mature sperm

Jovenal T. San Agustin[a], Gregory J. Pazour[a], and George B. Witman[b]
[a]Program in Molecular Medicine, University of Massachusetts Medical School, Worcester, MA 01605; [b]Department of Cell and Developmental Biology, University of Massachusetts Medical School, Worcester, MA 01655

ABSTRACT ***Drosophila*** **sperm are unusual in that they do not require the intraflagellar transport (IFT) system for assembly of their flagella. In the mouse, the IFT proteins are very abundant in testis, but we here show that mature sperm are completely devoid of them, making the importance of IFT to mammalian sperm development unclear. To address this question, we characterized spermiogenesis and fertility in the *Ift88*^{Tg737Rpw} mouse. This mouse has a hypomorphic mutation in the gene encoding the IFT88 subunit of the IFT particle. This mutation is highly disruptive to ciliary assembly in other organs. *Ift88*$^{-/-}$ mice are completely sterile. They produce ~350-fold fewer sperm than wild-type mice, and the remaining sperm completely lack or have very short flagella. The short flagella rarely have axonemes but assemble ectopic microtubules and outer dense fibers and accumulate improperly assembled fibrous sheath proteins. Thus IFT is essential for the formation but not the maintenance of mammalian sperm flagella.**

Monitoring Editor
Wallace Marshall
University of California, San Francisco

Received: Aug 17, 2015
Revised: Sep 23, 2015
Accepted: Sep 24, 2015

INTRODUCTION

Intraflagellar transport (IFT) is essential for the assembly and maintenance of most eukaryotic cilia and flagella (reviewed in Rosenbaum and Witman, 2002; Scholey, 2003). During IFT, large particles are transported along the axonemal microtubules from the cell body to the tip of the flagellum and then back to the cell body, where there is a large pool of IFT particles. The IFT particles carry cargo for assembly and maintenance of cilia and flagella (Piperno *et al.*, 1996; Hou *et al.*, 2007; Wren *et al.*, 2013; Craft *et al.*, 2015) and also carry signals between the cilium and the cell body (Pan and Snell, 2003; Goetz and Anderson, 2010; Keady *et al.*, 2012; Liem *et al.*, 2012; Eguether *et al.*, 2014).

The anterograde, base-to-tip movement of IFT particles is propelled by the microtubule motor kinesin-2 (Kozminski *et al.*, 1995; Scholey, 1996). In *Caenorhabditis elegans*, a second kinesin (OSM-3) cooperates with heterotrimeric kinesin-2 in this process (Ou *et al.*, 2005). The movement of particles back to the base of the axoneme is driven by cytoplasmic dynein 2, also known as dynein 1b in invertebrates (Pazour *et al.*, 1999; Porter *et al.*, 1999). The IFT particles are composed of at least 16 polypeptides in IFT complex B (IFT-B; Cole *et al.*, 1998; Follit *et al.*, 2009) and six proteins in IFT complex A (IFT-A; Cole *et al.*, 1998; Mukhopadhyay *et al.*, 2010). IFT particles also are associated with another complex—the BBSome—which contains eight proteins and likely functions as a cargo adapter (Nachury *et al.*, 2007; Lechtreck *et al.*, 2009, 2013). These proteins are highly conserved throughout the eukaryotic kingdom (van Dam *et al.*, 2013).

IFT is essential for the assembly of motile cilia in *Chlamydomonas* (Kozminski *et al.*, 1995; Pazour *et al.*, 1998, 1999, 2000; Brazelton *et al.*, 2001), *Tetrahymena* (Brown *et al.*, 1999), *Trypanosoma* (Davidge *et al.*, 2006; Absalon *et al.*, 2008), and sea urchin (Morris and Scholey, 1997) and for assembly of dendritic cilia in *C. elegans* (Collet *et al.*, 1998; Signor *et al.*, 1999; Wicks *et al.*, 2000) and *Drosophila melanogaster* (Han *et al.*, 2003; Sarpal *et al.*, 2003). In vertebrates, IFT also is required for assembly of motile (Banizs *et al.*, 2005; Kramer-Zucker *et al.*, 2005; Gilley *et al.*, 2014) and neuronal cilia (Davenport *et al.*, 2007), along with photoreceptor outer segments and other sensory cilia (Marszalek *et al.*, 2000; Pazour *et al.*, 2002; Tsujikawa and Malicki, 2004), of nodal and other embryonic cilia (Nonaka *et al.*, 1998; Marszalek *et al.*, 1999; Murcia *et al.*, 2000; Bangs *et al.*, 2015), and of kidney, pancreatic, and skin primary

This article was published online ahead of print in MBoC in Press (http://www.molbiolcell.org/cgi/doi/10.1091/mbc.E15-08-0578 on September 30, 2015.

Address correspondence to: George B. Witman (George.Witman@umassmed.edu), Gregory J. Pazour (Gregory.Pazour@umassmed.edu).

Abbreviations used: BSA, bovine serum albumin; DAPI, 4′,6-diamidino-2-phenylindole dihydrochloride; IFT, intraflagellar transport; IFT-A, IFT complex A; IFT-B, IFT complex B; ORPK, Oak Ridge Polycystic Kidney; PAS, Periodic acid-Schiff; PBS, phosphate-buffered saline; PVDF, polyvinylidene fluoride; TBST, Tris-buffered saline with Tween; TLCK, tosyl lysine chloromethyl ketone; TPCK, tosyl phenylalanyl chloromethyl ketone.

Supplemental Material can be found at:
http://www.molbiolcell.org/content/suppl/2015/09/28/mbc.E15-08-0578v1.DC1.html

cilia (Pazour *et al.*, 2000; Cano *et al.*, 2004; Lehman *et al.*, 2009). IFT also is necessary for the maintenance of flagella in *Chlamydomonas* (Kozminski *et al.*, 1993; Engel *et al.*, 2012; Witman, 2012).

In contrast to the importance of IFT for the assembly of cilia in most somatic tissues, *Plasmodium falciparum* has flagellated gametes, yet lacks IFT genes. In this species, it is believed that axonemal assembly occurs in the cytoplasm and the axoneme does not become membrane enclosed until after assembly (Avidor-Reiss *et al.*, 2004). Although IFT is needed for assembly of sensory cilia in *D. melanogaster*, it is dispensable for sperm flagellar assembly in this organism also. In *Drosophila*, it is believed that the sperm axoneme is assembled in the cytoplasm and, as in *Plasmodium*, does not become membrane enclosed until after assembly (Han *et al.*, 2003; Sarpal *et al.*, 2003). The observation that germ cell flagellar assembly does not require IFT in at least two species raises the question of whether IFT is necessary for the assembly and maintenance of the mammalian sperm flagellum. A study found that depletion of Kif3A, a subunit of kinesin-2, caused abnormalities in sperm head and tail development (Lehti *et al.*, 2013); however, Kif3A is involved in a number of cellular processes, including membrane organelle transport and microtubule dynamics (Yamazaki *et al.*, 1995; Boehlke *et al.*, 2013), so these effects cannot be attributed specifically to defective IFT.

In the mouse, complete knockout of an IFT motor or particle protein causes embryonic lethality (Nonaka *et al.*, 1998; Marszalek *et al.*, 1999). However, the *Oak Ridge Polycystic Kidney* (*orpk*) insertional mutation of the *Ift88* gene (Moyer *et al.*, 1994), which encodes the IFT-B protein IFT88 (Murcia *et al.*, 2000; Pazour *et al.*, 2000), is hypomorphic and is reported to result in expression of what may be an alternatively spliced mRNA (Moyer *et al.*, 1994; Taulman *et al.*, 2001) and a reduced amount of a smaller-than-normal IFT88 protein (Taulman *et al.*, 2001). This apparently supports sufficient residual IFT to allow the embryo to pass through critical stages in its development, so that some mice homozygous for the mutation survive to birth and even reach adulthood. Nevertheless, cilia formation in several neonatal and adult tissues is severely impaired. As a result, the mice have been very useful for investigating the role of cilia and IFT in these tissues (Pazour *et al.*, 2000, 2002; Cano *et al.*, 2004).

In this study, we examine the role of IFT in mouse sperm development. Sperm development begins with the formation of spermatogonia from germ-line stem cells. These cells undergo meiosis to become haploid spermatids. The spermatids then assemble cilia that undergo extensive modifications to form the mature sperm flagella. Previous work showed that IFT88 is expressed in testis (Taulman *et al.*, 2001) and is required for proper sperm tail assembly and morphogenesis of the sperm head (Kierszenbaum *et al.*, 2011). We extend these studies to characterize the timing of IFT88 expression in the testis, the detailed effect of IFT88 depletion on spermiogenesis, and the potential role of IFT in mature sperm. We find that although IFT proteins are critical for sperm development, they are not present in mature sperm and thus are not needed for sperm maintenance.

RESULTS

IFT-particle proteins are lacking from epididymal sperm but are highly expressed in testis

In a previous study using an anti-IFT88 antibody and immunofluorescence microscopy, it was reported that IFT88 was present in mature flagellated mouse sperm, where it was concentrated in the basal body region, with lesser amounts in the axoneme (Taulman *et al.*, 2001). To determine whether this was true also for other IFT-particle proteins, we isolated sperm from the epididymis and analyzed them by Western blotting. To our surprise, we were unable to detect either IFT-A (IFT140) or IFT-B (IFT88, IFT57, and IFT20) proteins in the epididymal sperm (Figure 1A).

To confirm that IFT proteins are expressed in testes (Taulman *et al.*, 2001), we did Northern blot analysis of RNA isolated from mouse tissues; the blots showed that testis had high IFT88 expression relative to other tissues (Figure 1B). Western blot analysis confirmed the high level of IFT88 expression in testis (Figure 1C). This suggests that IFT is important for sperm development but not needed in mature sperm.

We next investigated how the *Ift88*^{Tg737Rpw} hypomorphic mutation (Moyer *et al.*, 1994) affects testicular expression of IFT88 and other IFT-particle proteins and their assembly into IFT-A and IFT-B complexes. Compared to wild type, IFT88 protein is greatly reduced, but not completely missing, in testis of mice homozygous for the *Ift88*^{Tg737Rpw} mutation (hereafter abbreviated *Ift88*$^{-/-}$; Figure 1C). The remaining protein appears to be full length, and, in contrast to Kierszenbaum *et al.* (2011), we did not detect any smaller forms in mutant testis with our antibody directed against the C-terminal end of the protein. Mouse IFT-B proteins IFT88, IFT57, IFT52, and IFT20 sediment as a 17S particle in sucrose density gradients (Pazour *et al.*, 2002), indicating that these proteins form a large complex in the mouse, just as their homologues do in *Chlamydomonas* (Cole *et al.*, 1998). To determine how the *Ift88* mutation affects this complex, we compared sedimentation properties of the IFT particle from control and mutant testis (Figure 1D). In the gradient of the wild-type extract, IFT-B, represented by IFT88, IFT57, and IFT20, migrated at ~17S, as expected; IFT-A, represented by IFT140, sedimented slightly more slowly. Of importance, the particles from the mutant testes sedimented with properties similar to those from the wild-type testes. The residual IFT88 present in the mutant testis sedimented with the other IFT-B proteins, indicating that it is integrated into IFT-B. However, in the mutant, the amounts of IFT57 and IFT20 in IFT-B are in vast excess over the amount of IFT88. This suggests that a relatively intact IFT-B particle is assembled even when there is inadequate IFT88 to be incorporated into all the particles.

Mouse spermatogenesis and timing of IFT88 gene expression in testis

Previously spermatogenesis was carefully examined in the rat (Leblond and Clermont, 1952; Russell *et al.*, 1990). Although mouse spermatogenesis has not been so thoroughly characterized, Russell *et al.* (1990) built on the existing literature for both rat and mouse to provide a very useful description of the events during mouse spermiogenesis. To assist in interpreting the effects of the *Ift88* mutation on sperm development, we have combined the diagrams of Russell *et al.* (1990) with our observations to order the key steps of flagellar development during mouse spermiogenesis (Figure 2). Spermatogenesis, or the development of sperm, begins with germ cells dividing and undergoing meiosis to generate spermatids. These develop into spermatozoa through the process of spermiogenesis. Spermiogenesis can be divided into 16 steps (Arabic numerals in Figure 2), which occur in synchronous waves along the seminiferous tubules of the testes. A section through a tubule will reveal germ cells at three or four stages of spermatogenesis, with one or two of these being spermiogenic. The more mature cells are organized in a band near the central lumen, and progressively less mature cells are localized in zones progressively closer to the outer surface or boundary of the tubule. Twelve distinct morphologies of the tubule (called stages and written in Roman numerals) can be distinguished by the steps of development occurring in a given tubule cross-section. For example, a section through a stage IV tubule will reveal step 15 spermatids with their flagella extending into the lumen of the tubule and

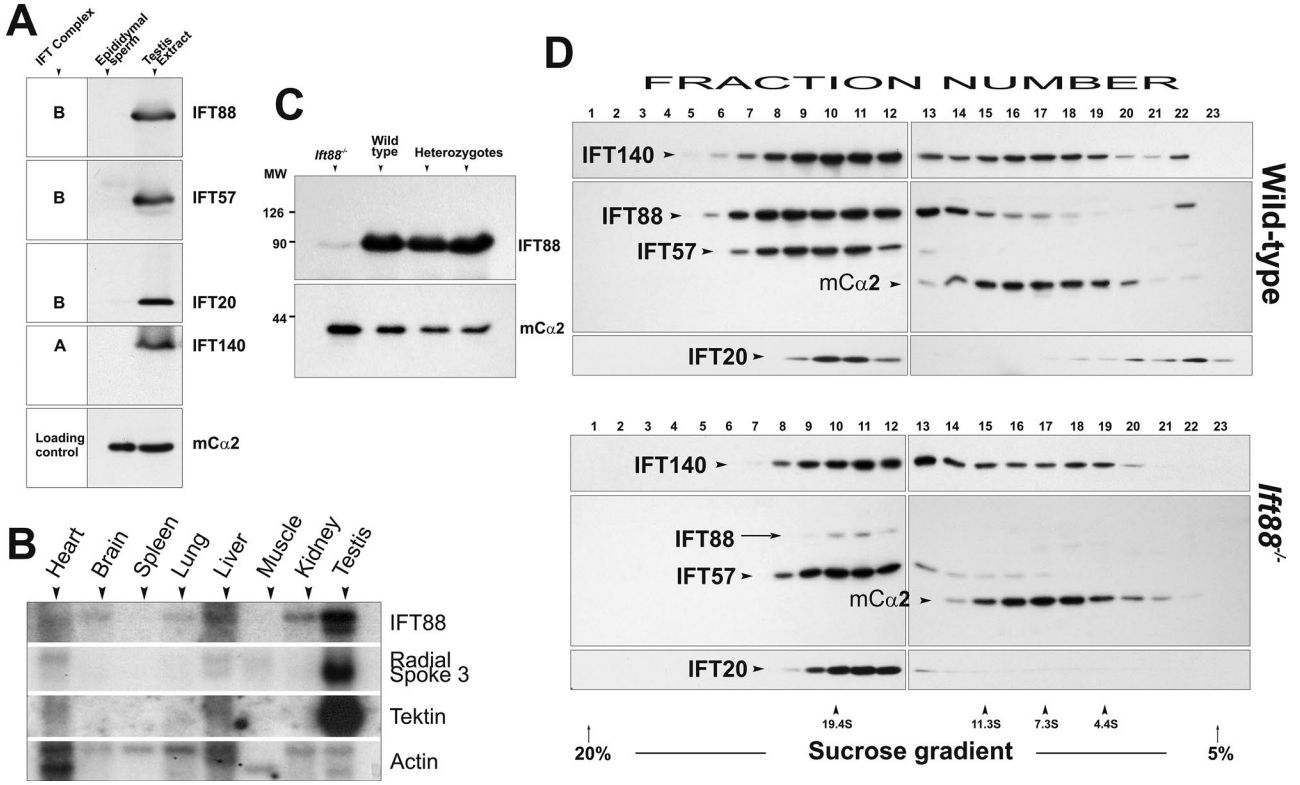

FIGURE 1: IFT88 expression in wild-type and *Ift88*$^{-/-}$ testes. (A) Western blots of wild-type testis and epididymal sperm extracts probed with antibodies to the indicated IFT-A and IFT-B proteins and to Cα_2, the testis-specific isoform of the catalytic subunit of cAMP-dependent protein kinase. IFT proteins are readily detected in testis extract but are not found in epididymal sperm. The blot was stripped and reprobed with an antibody to Cα_2 to confirm that comparable amounts of sperm protein were loaded in each lane. (B) Northern blot of wild-type mouse tissues probed with cDNAs encoding IFT88, radial spoke protein 3, tektin, and actin. IFT88 mRNA is most highly expressed in testis, with lower levels of expression in kidney, liver, lung, and brain. Tektin and radial spoke protein 3, components of ciliary and flagellar axonemes, also are most highly expressed in testis. In contrast, actin is expressed in all tissues. (C) Top, Western blot of IFT88 protein in testis extracts. The anti-IFT88 antibody recognizes a single protein of ~90 kDa, which agrees well with the predicted mass of 92.9 kDa for IFT88, in homozygous *Ift88*$^{-/-}$ (–/–), wild-type (+/+), and heterozygous (+/–) mice, but the amount of protein in the mutant mouse testis is much lower than in the wild-type or heterozygous testes. Bottom, the same blot stripped and reprobed with the anti-Cα_2 antibody as a loading control. (D) Western blots of fractions from sucrose density gradients loaded with testis extracts from wild-type (top) and *Ift88*$^{-/-}$ (bottom) mice; the blots were probed with antibodies to an IFT-A protein (IFT140), IFT-B proteins (IFT88, IFT57, IFT20), and Cα_2. In the gradient of wild-type testis extract, IFT88, IFT57, and IFT20 cosediment at ~17S, whereas IFT140 sediments slightly more slowly. In the gradient of mutant testis extract, there is about the same amount of IFT140, IFT57, and IFT20 as in wild type, but the amount of IFT88 is greatly reduced. Nevertheless, all three IFT-B proteins cosediment at ~17S. The blots were probed for Cα_2 as a control to confirm that equivalent amounts of wild-type and *Ift88*$^{-/-}$ extracts were loaded on the sucrose gradients.

step 4 spermatids located in a band between the lumen and the outer surface of the tubule. Spermiogenesis begins at step 1 with the appearance of haploid, round spermatids arising from two sequential meiotic divisions of the diplotene spermatocytes. During step 2-3, the 9 + 2 flagellar axoneme begins to elongate from a basal body located just below the plasma membrane and reaches nearly full length (Irons and Clermont, 1982). At this time, the axoneme is tightly surrounded by the flagellar membrane, which is continuous with cellular plasma membrane. Also during step 2-3, the precursors or "anlagen" of the fibrous sheath columns begin to form at the distal end of the flagellum (Sakai *et al.*, 1986). The fibrous sheath columns and ribs subsequently are assembled in a distal-to-proximal direction in what will become the principal piece of the sperm (Irons and Clermont, 1982). Between steps 6 and 7 (Russell *et al.*, 1990), the basal body with attached axoneme migrates inward to the nucleus and pulls the plasma membrane along with it to create an invagination of the plasma membrane that now surrounds the proximal portion of the flagellum. At step 8, the outer dense fibers begin to form at the proximal end of the axoneme. The fibers assemble along the axonemal doublet microtubules in a proximal-to-distal direction, eventually extending the entire length of the midpiece and principal piece but not reaching their full diameter until step 16. At step 9, the nucleus begins to elongate and condense. Also at this step, the annulus—a septin-based ring of dense material—starts to form and surrounds the axoneme at its base (Guan *et al.*, 2009). At step 15, the annulus migrates distally along the axoneme to the future site of the midpiece/principal piece junction (Guan *et al.*, 2009; Kwitny *et al.*, 2010). The axoneme and outer dense fibers proximal to this site are now surrounded by the spermatid's caudal cytoplasm and will become the midpiece. Beginning

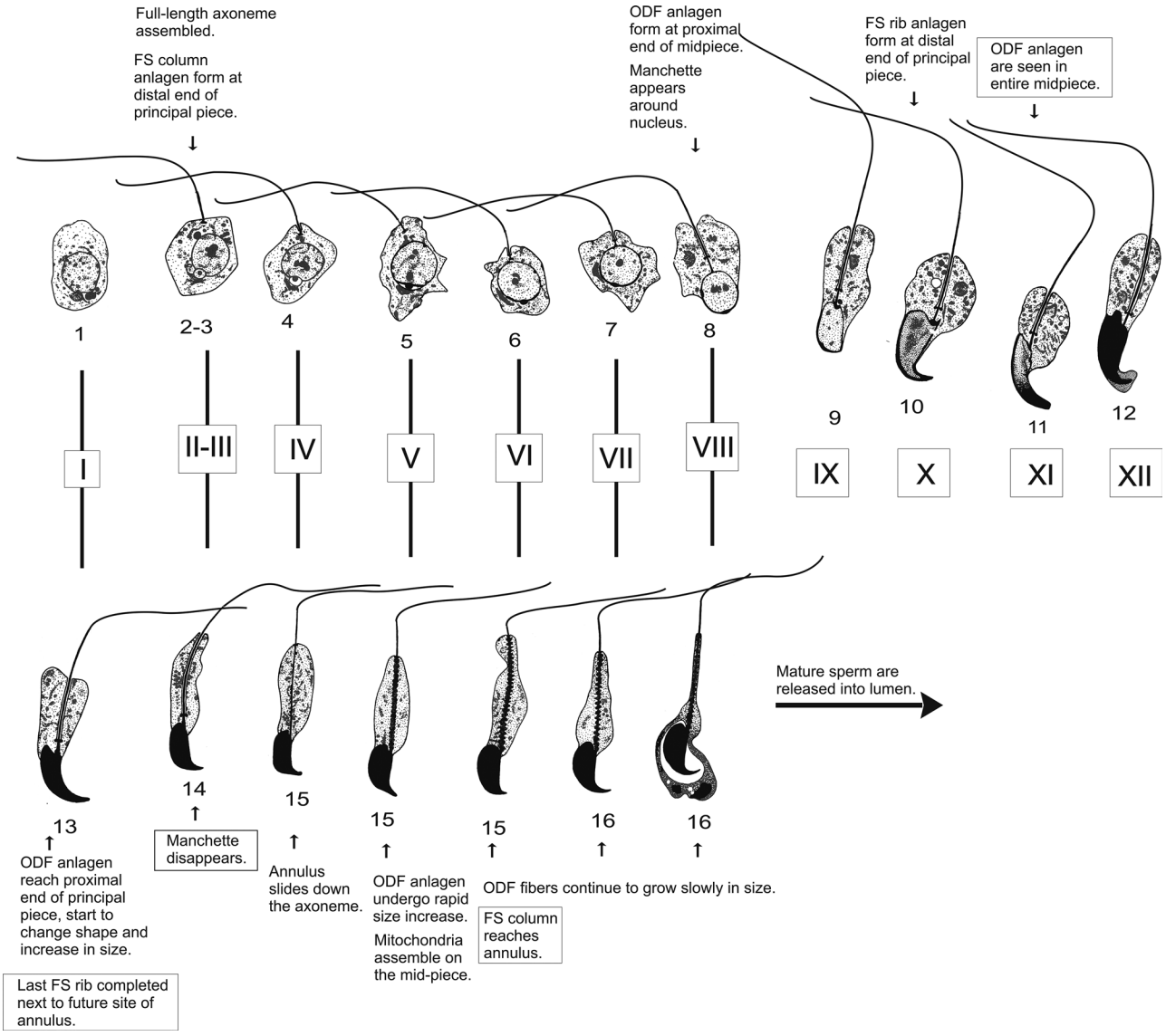

FIGURE 2: Key steps in the development of the mouse sperm flagellum during spermiogenesis. Adapted from Russell *et al.* (1990). Boxed events were determined from our experiments unless stated otherwise. Steps 1–8 are round spermatids, before the beginning of nuclear condensation and elongation in step 9. Based on the rat (Leblond and Clermont, 1952; Russell *et al.*, 1990), the axoneme is assembled to full length in step 2-3. Assembly of outer dense fibers (ODFs) around the axoneme begins at the proximal end of the midpiece of step 8 spermatids; the process is completed just before the mature sperm is released into the lumen of the seminiferous tubule. Fibrous sheath (FS) assembly begins at the distal end of the principal piece of step 2 rat spermatids with the formation of fibrous sheath columns along the axonemal doublet microtubules 3 and 8; a similar event is presumed to take place in step 2-3 mouse spermatids. Assembly of fibrous sheath ribs on the columns starts in step 10 spermatids and is complete in step 13 spermatids. The manchette is first seen in step 8 spermatids and disappears by step 14. The annulus slides distally down the axoneme to its final location between the distal end of the midpiece and the proximal end of the principal piece when step 15 is reached (Kwitny *et al.*, 2010). The mitochondria then condense along the length of the midpiece.

at step 15, mitochondria in the developing midpiece migrate to the axoneme and condense around the axoneme and outer dense fibers (Russell *et al.*, 1990). In step 16, the flagellar membrane becomes closely opposed to the mitochondrial sheath in the midpiece and the excess cytoplasm is eliminated as the residual body (O'Donnell *et al.*, 2011). Mature sperm are then released into the lumen and exit the testis.

To determine when and where during spermatogenesis IFT88 is expressed in testis, we used immunofluorescence microscopy of sections through wild-type seminiferous tubules (Figure 3A). We found that IFT88 was first apparent in pachytene spermatocytes of stage II-III (Figure 3Aa) and was strongly labeled in pachytene cells at stage VIII (Figure 3Ab). It continued to be expressed as the spermatocytes underwent maturation, as shown by its presence in the tails of developing spermatids at both of these stages (Figure 3A, a, and b).

Because most sections of spermatogenic tubules contain spermatids in more than one stage (e.g., the stage II-III section

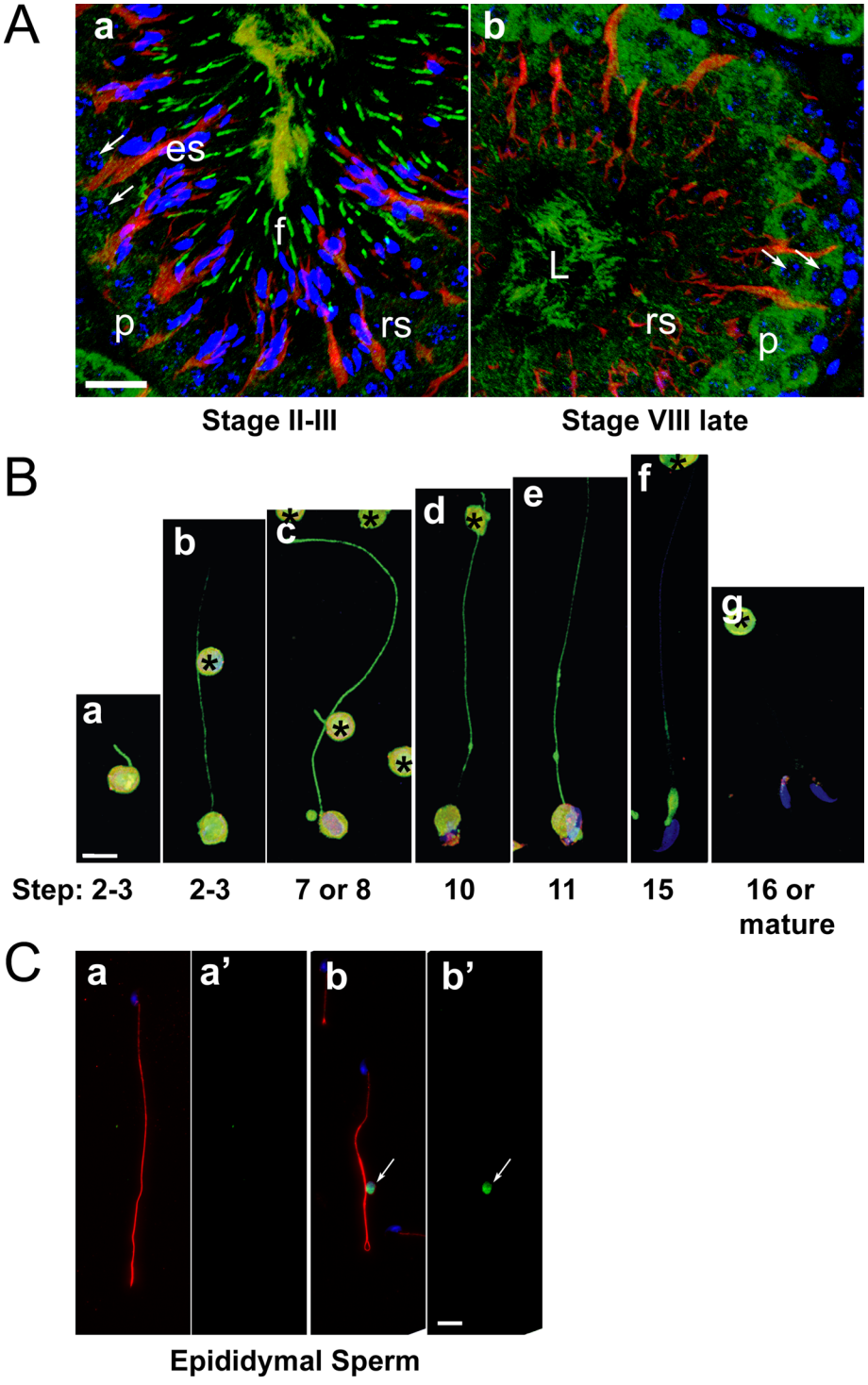

FIGURE 3: Timing and location of IFT88 expression in wild-type testis. (A) Immunofluorescence micrographs of sections through (a) stage II-III and (b) stage VIII seminiferous tubules labeled with anti-IFT88 antibody (green), anti–α-tubulin (red), and the nuclear stain TOTO-3 (blue). Arrows point out pachytene cell nuclei, in which the chromatin is condensed into multiple distinct foci; in a, IFT88 is just beginning to appear in the cytoplasm surrounding the pachytene nuclei. The bright red tubulin labeling marks Sertoli cells, through which the developing spermatids pass. es, elongated spermatids; f, flagella; L, lumen; p, pachytene; rs, round spermatids. Scale bar, 20 μm. (B) Immunofluorescence micrographs of individual isolated spermatids labeled with anti-IFT88 (green), anti–α-tubulin (red), and TOTO-3 (blue). (a) The round head and short flagellum suggests that this is an early step 2-3 spermatid. (b) The round head and longer flagellum indicates that this is a step 2-3 or slightly later spermatid. (c) The nucleus has just begun to elongate, but the head is round and lacks a cytoplasmic lobe, indicating that this is a step 7 or possibly step 8 spermatid. (d) The more elongated shape of the head and nucleus and the distinct cytoplasmic lobe suggest that this is a step 10 spermatid. (e) The nucleus is highly condensed, and the head is more elongated than in d, suggesting that this is a step 11 spermatid. (f) The condensed nucleus, sharp narrow apex of the head, and presence of long narrow cytoplasmic lobe indicate that this is a later, probably step 15, spermatid. (g) The shape of the head (which is properly oriented to display the typical hook only in the spermatid on the right) and absence of cytoplasmic lobes suggest that these are either late step 16 spermatids that have already lost their cytoplasmic lobes or mature sperm from the tubule lumen. IFT88 labeling is present in the heads and tails of step 2-3 through 11 spermatids, limited largely to the cytoplasmic lobe in the step 15 spermatid, and no longer detected in the step 16 spermatids/mature sperm. Asterisks mark heads from other spermatogenic cells. Scale bar, 10 μm. (C) Immunofluorescence micrographs of epididymal sperm labeled with anti-acetylated α-tubulin (red), anti-IFT88 (green), and DAPI (blue). (a, b) Merged images; (a′, b′) just the green (IFT88) channel for the respective images. Tubulin labeling is readily apparent, but IFT88 is not detectable in the sperm head or tail. Although the distal part of the tail has doubled back on itself in the sperm shown in b and b′, the image shows what appears to be a cytoplasmic droplet (arrow) that serves as a positive control for the IFT88 labeling. Scale bar, 10 μm.

shown in Figure 3Aa contains spermatids in steps 2-3 and 14), it was difficult to determine conclusively whether IFT88 was localized to the tails of both early and late spermatids. To address this, we examined the distribution of IFT88 in isolated spermatids that could be identified with regard to step using the criteria of Russell *et al.* (1990; Figure 3B). The anti-IFT88 antibody strongly labeled the heads and developing flagella of step 2-3 through 11 spermatids (Figure 3B, a–e). At step 15, IFT88 labeling was less bright and concentrated in the cytoplasmic lobe and at the proximal end of the principal piece, suggesting that IFT winds down as the tail reaches maturity (Figure 3Bf). IFT88 labeling was not detected in cells that appeared to be either late step 16 spermatids or mature sperm that already had been released into the tubule lumen (Figure 3Bg).

To confirm that IFT88 was absent from fully formed sperm, we also examined sperm extruded from the caudal epididymides. Even using an antigen retrieval step similar to one used previously to enhance both IFT88 and tubulin labeling in the photoreceptor outer segment (Keady *et al.*, 2011),

Wild-type males	*Ift88*$^{-/-}$ males
Trial I,[a] 10/10 females pregnant (8.4 ± 1.3 pups/litter)	0/10 females pregnant (no pups)
Trial II,[b] 10/10 females pregnant (9.0 ± 3.3 pups/litter)	0/10 females pregnant (no pups)

[a]In Trial I, five wild-type and five Ift88$^{-/-}$ males were each mated to two wild-type females and litters scored during the fourth week. After 6 wk, males were separated from females for 3 wk.
[b]In Trial 2, the males were swapped so that females previously paired to Ift88$^{-/-}$ males were paired with control males and vice versa.

TABLE 1: Male fertility.

we detected no IFT88 in the epididymal sperm head or tail (Figure 3C).

Male *Ift88*$^{-/-}$ mice are sterile

To test the importance of IFT88 to male fertility, five wild-type and five *Ift88*$^{-/-}$ male mice were each mated to two wild-type female mice. All 10 females mated to wild-type males produced litters during week 4 (Table 1). In contrast, although the females mated to *Ift88*$^{-/-}$ male mice were plugged, none became pregnant. All mice were then rested for 3 wk, and the females that originally had been mated to the mutant mice were mated to wild-type mice and vice versa. Again, all females mated to wild-type males produced litters, confirming that they were fertile. However, the females mated to the mutant males failed to produce litters, indicating that *Ift88*$^{-/-}$ male mice are sterile. In contrast, female *Ift88*$^{-/-}$ mice are fertile (McDermott *et al.*, 2010).

To understand the origin of male infertility in the *Ift88*$^{-/-}$ mice, we extruded the contents of the cauda epididymides into phosphate-buffered saline (PBS) and examined them by light microscopy. The mean total count (heads plus tails plus heads with tails) for mutant mice was ~350 times lower than for wild-type animals (Table 2). The tails of wild-type sperm beat slowly, whereas those of the *Ift88*$^{-/-}$ sperm were completely immotile. Wild-type sperm had well-shaped heads and long, smoothly tapering flagella, whereas the mutant sperm were morphologically abnormal (Figure 4A). The mutant sperm heads often lacked flagella entirely, and when a flagellum was present, it was always short and misshapen.

The reduced sperm production was confirmed by periodic acid-Schiff (PAS)-hematoxylin–stained sections of wild-type and *Ift88*$^{-/-}$ testes. Mutants showed a reduced number of condensed spermatid nuclei in the epithelium and a distinct absence of flagella in the lumen of the seminiferous tubules (Figure 4B). In addition, the sperm heads were not uniformly located at the edge of the lumen of the *Ift88*$^{-/-}$ tubules as they are in controls (Figure 4B). The very low sperm count, abnormal sperm morphology, and lack of sperm motility undoubtedly account for the infertility of the *Ift88*$^{-/-}$ mice.

	Sperm count
Wild type	19,000,000 ± 2,600,000
Ift88$^{-/-}$	56,000 ± 31,000 ($p \leq 0.0001$)

Sperm count included heads with tails, heads without tails, and tails without heads if present. Three mutants and six control males were harvested at >8 wk of age.

TABLE 2: Epididymal sperm count.

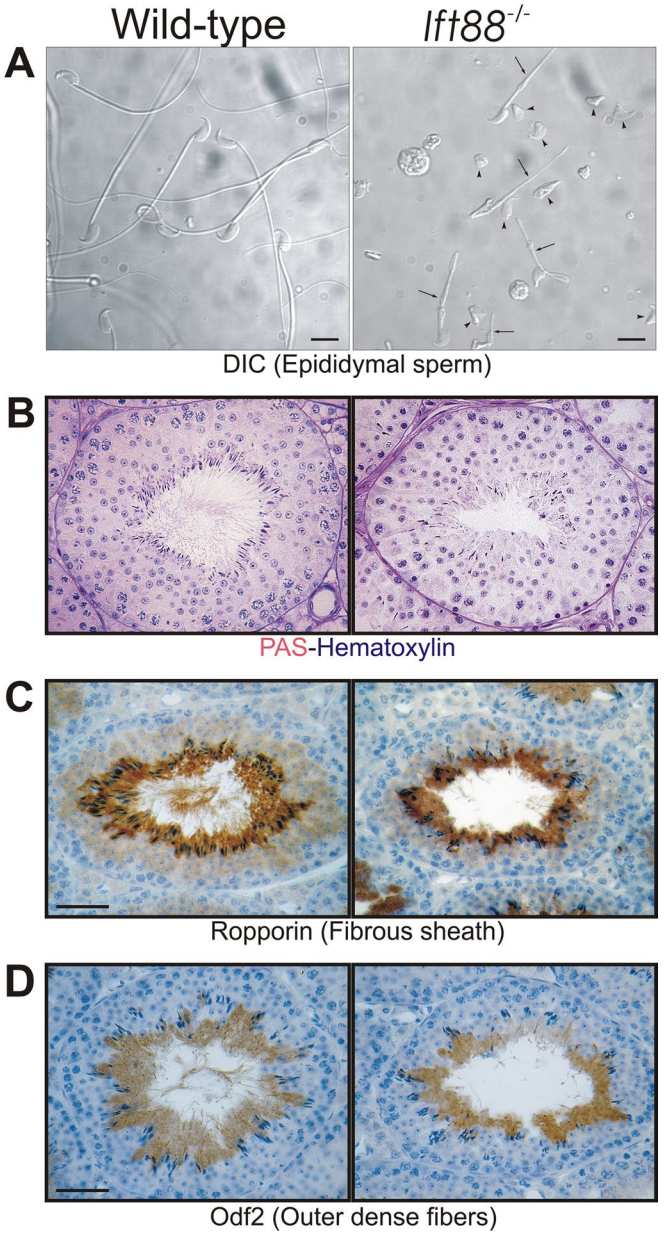

FIGURE 4: Comparison of wild-type and *Ift88*$^{-/-}$ sperm and seminiferous tubules. (A) Differential interference contrast micrographs of wild-type and *Ift88*$^{-/-}$ epididymal sperm. Wild-type sperm have well-shaped heads and long, gradually tapering tails. The *Ift88*$^{-/-}$ epididymal exudate contained numerous sperm heads without tails (arrowheads); when heads did have tails, the tails were short and abnormally shaped (arrows). Many *Ift88*$^{-/-}$ sperm heads also were misshapen. Scale bars, 10 µm. (B) PAS- and hematoxylin-stained sections of stage VII seminiferous tubules. Flagella were present in the lumen of the wild-type tubule but absent from the lumen of a comparable *Ift88*$^{-/-}$ tubule. The spermatid nuclei are fewer in number and not as well aligned along the edge of the lumen in the *Ift88*$^{-/-}$ tubule. (C) Sections of stage VII tubules. Antibodies against the fibrous sheath component ropporin (brown) strongly stained the cytoplasm of both wild-type and *Ift88*$^{-/-}$ step 16 spermatids and the flagella of wild-type step 16 spermatids. Sections were counterstained with hematoxylin (blue). (D) Sections of stage IV-V tubules. Antibodies against the outer dense fiber component Odf2 (brown) stained the cytoplasm of both wild-type and *Ift88*$^{-/-}$ step 15 spermatids and the flagella of wild-type step 15 spermatids. Sections were counterstained with hematoxylin (blue). Ropporin and Odf2 labeling in tubules of additional stages are shown in Supplemental Figures S1–S4. Scale bar, 20 µm.

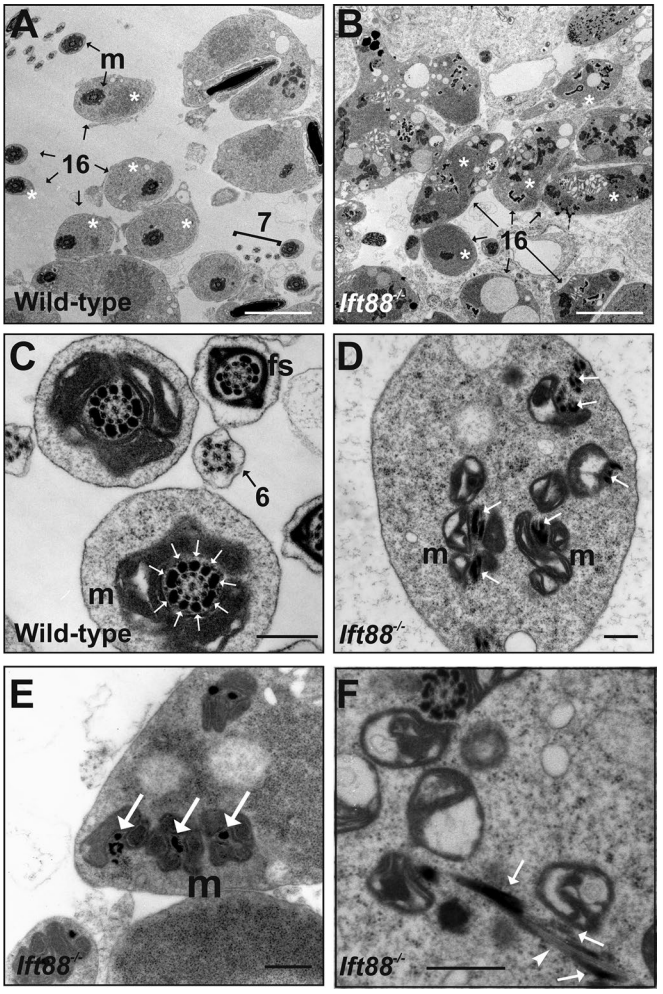

FIGURE 5: The caudal cytoplasm of *Ift88*$^{-/-}$ spermatids often lack axonemes and have ectopically assembled outer dense fibers. (A) Electron micrograph of a section tangential to the lumen of a wild-type stage VII seminiferous tubule. This micrograph contains cross-sections through the caudal cytoplasm, or developing midpieces, of several step 16 spermatids (16, asterisks). The midpieces decrease in diameter as the cross-sections are cut closer to the junction with the principal piece. Virtually every midpiece contains an axoneme with outer dense fibers around which the midpiece mitochondria (m) have condensed. Also seen are cross-sections through the principal pieces of several less mature step 7 (7) spermatids, all of which contain axonemes. Scale bar, 5 μm. (B) A comparable section through the caudal regions of several *Ift88*$^{-/-}$ step 16 spermatids (16) showing cross-sections of what should be developing midpieces (asterisks). In contrast to the wild-type section, not a single normal axoneme is apparent in these "midpieces," although axonemes were occasionally seen in other sections. Normal principal pieces also are not seen. Scale bar, 5 μm. (C) A higher magnification of cross-sections through the midpiece region of two wild-type step 16 (tubular stage VI) spermatids in which mitochondria (m) have condensed around the outer dense fibers (white arrows), one of which is associated with each of the nine axonemal doublet microtubules. Also visible are flagella of step 6 round spermatids (6), which have not yet assembled outer dense fibers, and a principal piece of a step 16 spermatid, which has a fibrous sheath (fs). Scale bar, 500 nm. (D) A section through the developing "midpiece" of an *Ift88*$^{-/-}$ step 16 spermatid. No axoneme is present. Numerous outer dense fibers (white arrows) are scattered throughout the cytoplasm and are serving as foci for condensation of midpiece mitochondria (m). Scale bar, 500 nm. (E) Enlarged image of the developing "midpiece" of another *Ift88*$^{-/-}$ step 16 spermatid. Mitochondria (m) have condensed around several ectopically located outer dense fibers (white arrows). Scale bar, 500 nm. (F) A section through the midpiece of an *Ift88*$^{-/-}$ step 16 spermatid, showing one of the few instances in which an axoneme was observed. Even in the presence of an axoneme and its associated outer dense fibers, some outer dense fibers have assembled ectopically (white arrows) in the cytoplasm. A microtubule (arrowhead) is associated with one or more of the outer dense fibers. Scale bar, 500 nm.

Expression of representative sperm flagella structural proteins is normal in *Ift88*$^{-/-}$ testes

To determine the effect of reduced IFT88 on the expression of structural proteins necessary for the development of sperm flagella, we used immunohistochemistry to evaluate production and localization of the fibrous sheath rib component ropporin (Fujita *et al.*, 2000) and the outer dense fiber component Odf2 (Hoyer-Fender *et al.*, 1998). In the wild-type testis, ropporin is first detected in the cytoplasm of step 4 round spermatids and begins to be incorporated into the flagella in step 9 spermatids (Supplemental Figure S1). Staining also is observed in the residual bodies that are resorbed by the Sertoli cells in stage VIII seminiferous tubules. In mutant testes, the staining pattern was similar, except that few flagella were observed in the seminiferous tubules (Supplemental Figure S2). However, when flagella were present, they were stained by the anti-ropporin antibodies (Figure 4C).

Odf2 was initially seen in the cytoplasm of step 12 elongate spermatids (Supplemental Figure S3). Odf2 staining became detectable in the flagella of step 13 elongate spermatids and was most intense in the cytoplasm and flagella of step 15 spermatids. These data suggest that there is a substantial lag between the synthesis of Odf2 mRNA, which is reported to begin in step 5 spermatids and peak in step 10/11 elongating spermatids (Hoyer-Fender *et al.*, 1998), and the appearance of Odf2 protein. Subsequently the Odf2 protein is moved into the flagella of step 16 spermatids; very little appeared to be resorbed in the residual bodies. In *Ift88*$^{-/-}$ testis, the few flagella that formed were positive for Odf2 (Figure 4D). Of interest, even though most Odf2 was not incorporated into flagella in the mutant, Odf2 label disappeared by step 15 (Supplemental Figure S4), suggesting that the excess protein was broken down. Thus, even though sperm development is greatly altered by the reduction in amount of IFT88, the timing and pattern of expression of important fibrous sheath rib and outer dense fiber components are not noticeably altered.

Axonemal growth is truncated while microtubules and accessory structure components accumulate in *Ift88*$^{-/-}$ spermatid flagella

To learn more about the morphological defects in *Ift88*$^{-/-}$ sperm, we carried out ultrastructural analysis of developing spermatids. Stage VI–VIII tubules, which contain spermatids at steps 6–8 and steps 15 and 16, are particularly informative for examining fibrous sheath and outer dense fiber assembly.

Cross-sections through the caudal cytoplasm of controls at these stages showed well- organized axonemes, which, at the later stages, were surrounded by outer dense fibers; in the developing midpiece, mitochondria were condensing around the axonemes and associated outer dense fibers (Figure 5, A and C). In contrast to the controls, most sections through the caudal cytoplasm of mutant sperm did not reveal any cross-sections of axonemes (Figure 5, B, D, and E); in these cells, the outer dense fibers formed ectopically in the

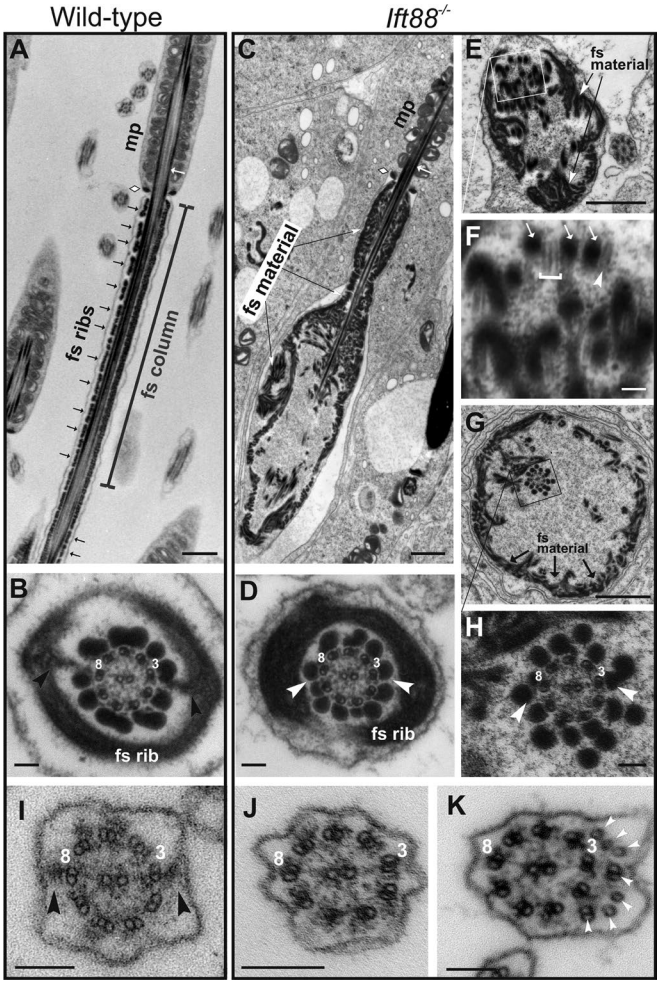

FIGURE 6: Principal pieces of *Ift88*$^{-/-}$ spermatids have truncated axonemes, lack fibrous sheath longitudinal columns, accumulate fibrous sheath rib material, and have numerous ectopically assembled outer dense fibers and microtubules. (A) Longitudinal section through the developing flagellum of a wild-type step 15 spermatid; the annulus (white diamond) marks the boundary between the midpiece (mp) and the principal piece, in which can be seen fibrous sheath ribs (black arrows) and a fibrous sheath longitudinal column (bracket) on either side of the axoneme. (B) A cross-section through the principal piece of a wild-type step 15 spermatid showing the fibrous sheath longitudinal columns (arrowheads) associated with doublets 3 and 8 and the fibrous sheath ribs that are attached to the longitudinal columns and surround the axoneme. (C) A longitudinal section through a *Ift88*$^{-/-}$ step 15 spermatid, comparable to the section of the wild-type spermatid shown in A; the boundary between the midpiece (mp) and the principal piece is marked by the annulus (white diamond). The end of the flagellum is swollen and filled with what appears to be unorganized fibrous sheath rib material. (D) Cross-section through the principal piece of an *Ift88*$^{-/-}$ step 15 spermatid showing an axoneme, which has two extra outer dense fibers but otherwise appears to be normal. The fibrous sheath ribs are present, but the longitudinal columns, which normally are associated with doublets 3 and 8, are missing (arrowheads). (E) Cross-section through a swollen principal piece of an *Ift88*$^{-/-}$ step 15 spermatid. No axoneme is present; numerous ectopically assembled outer dense fibers are visible, and a large amount of fibrous sheath rib material has accumulated around the periphery of the swollen flagellum. (F) A higher magnification of the boxed region in E. The outer dense fibers (arrows) are associated with singlet (arrowhead) or doublet (bracket) microtubules. (G) Another cross-section through the principal piece of an *Ift88*$^{-/-}$ spermatid. Although an axoneme is present, the fibrous sheath material remains associated with the distended flagellar membrane. (H) A higher magnification of the boxed region in G showing the axoneme, which lacks fibrous sheath longitudinal columns (arrowheads) and has supernumerary outer dense fibers. (I) Cross-section through a flagellum of a wild-type step 6 spermatid. The anlagen of the fibrous sheath longitudinal columns (black arrowheads) is visible adjacent to doublets 3 and 8. (J, K) Cross-sections through flagella of *Ift88*$^{-/-}$ probable step 6 spermatids. The anlagen of the fibrous sheath longitudinal columns are missing. The mutant flagellum in K has supernumerary singlet and doublet microtubules (white arrowheads). Scale bars, 1 μm (A, C, E, G), 100 nm (B, D, F, H–K).

cytoplasm and often had mitochondria associated with them. Even when an axoneme was present, outer dense fibers, sometimes associated with microtubules, were formed ectopically (Figure 5F).

To better understand how the reduction in IFT affected assembly of the axoneme and its accessory structures, we examined the principal pieces of the relatively rare *ift88*$^{-/-}$ spermatids that had a flagellum (Figure 6). In principal pieces of controls at step 6, outer dense fibers have not yet initiated, but the longitudinal columns of the fibrous sheath are formed and attached to doublets 3 and 8 (Figure 6I). At step 15, nine outer dense fibers are being assembled along the axoneme and will be completed in the next step. The fibrous sheath is completed at step 15 and consists of two longitudinal columns attached to outer doublets 3 and 8 and transverse ribs that form an arc around the axoneme, bridging the longitudinal columns (Figure 6, A and B). In principal pieces of the mutant, fibrous sheath assembly is defective from the earliest stages, and the longitudinal columns appear either to never form or never attach to the doublets (Figure 6, J and K). In some cases, the fibrous sheath rib material surrounded the outer dense fibers normally (Figure 6D), but in most cases, it condensed into large aggregates that were associated with the membrane (Figure 6, C, E, and G). Axonemes often were surrounded by supernumerary outer dense fibers (Figure 6, D and H); ectopic microtubules also were observed (Figure 6K). In some cross-sections of tails lacking an organized axoneme, large numbers of outer dense fibers were associated with singlet and doublet microtubules (Figure 6, E and F). In some *Ift88*$^{-/-}$ spermatids, the distal end of the flagellum was greatly swollen, suggesting an accumulation of unassembled axonemal precursors (Figure 6, C and G). Axonemes in the mutant flagella appeared to have a normal complement of inner and outer dynein arms and radial spokes (Figure 6, D, H, J, and K).

Nuclear reshaping of *Ift88*$^{-/-}$ spermatids is impaired

Normally, in late development, sperm nuclear chromatin condenses and the head undergoes an elongation event that forms the mature structure. This process can be seen in wild-type spermatids at step 11 (Figure 7A). Although *Ift88*$^{-/-}$ mutant cells undergo chromatin condensation and head elongation, many of the heads are abnormally shaped, as previously reported (Kierszenbaum *et al.*, 2011; Figure 7B). At the electron microscopic level, control step 11 spermatids have partially condensed and elongated nuclei capped by the acrosome (Figure 7D). In addition, just distal to the acrosome, the nucleus is surrounded by the microtubular manchette. The anterior ends of the manchette microtubules are embedded in the nuclear ring at the posterior edge of the acrosome, and the microtubules extend posteriorly parallel to the elongating nucleus, ending in scattered electron densities in the caudal cytoplasm of the spermatid. Equivalent electron micrographs of *Ift88*$^{-/-}$ step 11 spermatids revealed abnormally shaped nuclei that are tipped by

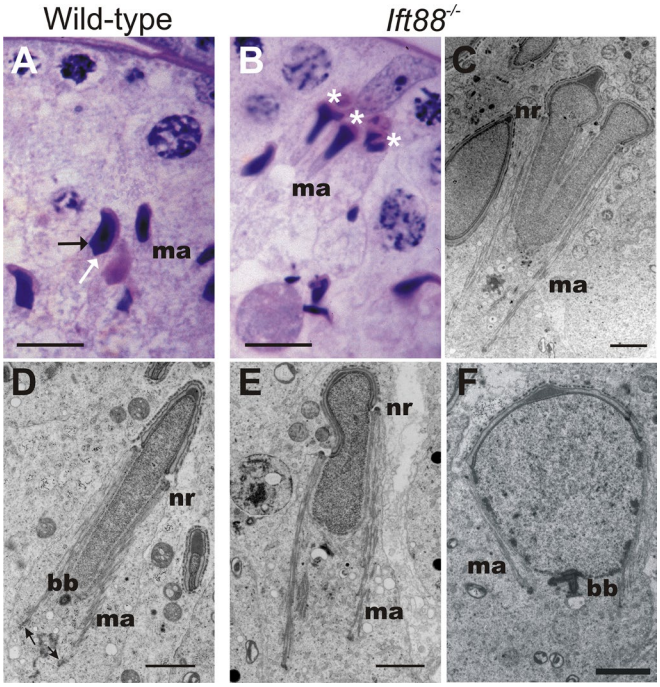

FIGURE 7: Nuclear shaping is defective in *Ift88*$^{-/-}$ spermatids. (A) Histological section of a wild-type stage XI seminiferous tubule. The nuclei of the step 11 spermatids have elongated; the ventral and dorsal angles (black and white arrows, respectively) are visible on some of the nuclei. (B) A comparable section through an *ift88*$^{-/-}$ stage XI seminiferous tubule. Although the nuclei are elongated, several have abnormal shapes (asterisks). (C) Electron micrograph of an *ift88*$^{-/-}$ step 11 spermatid in which the nucleus appears to be nearly bifurcated by an invagination of cytoplasm containing manchette microtubules (ma), which insert into typical electron densities at both their proximal and distal ends. (D) Electron micrograph of a wild-type step 11 spermatid showing the nucleus, basal body (bb), and manchette; the manchette microtubules (ma) insert into the nuclear ring (nr) at their proximal ends and into electron-dense material (arrows) at their distal tips. (E) Another example of an *ift88*$^{-/-}$ step 11 spermatid with distorted nuclei. ma, manchette microtubules; nr, nuclear ring. (F) An *ift88*$^{-/-}$ spermatid in which a manchette (ma) has formed and the centrioles are present adjacent to the nuclear envelope but no axoneme is observed and instead one of the centrioles (bb) appears to be capped by a vesicle. Scale bars, 10 μm (A, B), 2 μm (C–F).

malformed acrosomal caps (Figure 7, C and E). As in wild type, the anterior ends of the manchette microtubules are embedded in a nuclear ring, and the microtubules parallel the nuclear envelope, terminating in electron-dense material; however, the manchette, in concert with the nucleus, often is severely misshapen. Figure 7F illustrates a developing spermatid in which the manchette has formed and the centrioles are in contact with the nucleus. Normally, an axoneme would be present at this step, but here no axoneme is seen; instead, the centriole appears to be capped by a vesicle.

Ift88$^{-/-}$ spermatocytes and spermatids are eliminated by resorption and apoptosis

To understand the underlying cause of the reduced sperm count in the *Ift88*$^{-/-}$ mice, we compared the number of spermatocyte and spermatid nuclei in wild-type and mutant testes. Quantitative analysis revealed that the number of cells reaching the pachytene state in the mutant testis is about normal but that the number of round

	Preleptotene spermatocytes	Pachytene spermatocytes	Round spermatids
Wild type	12.5 ± 1.9	12.1 ± 1.7	45.5 ± 3.6
Ift88$^{-/-}$	11.3 ± 1.6 (ns)	11.5 ± 1.6 (ns)	32.9 ± 4.2 ($p \leq 0.05$)

Numbers indicate cells per 3-μm-thick seminiferous tubule cross-sections ± SD (see *Materials and Methods*). Three animals per genotype. Significance is compared with wild type at the same stage.

TABLE 3: Developing sperm cell count in seminiferous tubule cross-sections.

spermatids is only about two-thirds of the wild-type value (Table 3). At least some of this loss is due to apoptosis. In wild-type testes, apoptosis of spermatogonia is observed in late development (tubule stages IX–XII), but apoptosis of spermatocytes is rarely observed (Dym, 1994; Figure 8A). In contrast, in *Ift88*$^{-/-}$ testes, numerous terminal deoxynucleotidyl transferase dUTP nick end labeling (TUNEL)–positive spermatocytes at the late pachytene, diplotene, and metaphase stages were observed (Figure 8, B–D). Therefore loss of cells appears to begin after initiation of synthesis of IFT88 but before initiation of flagellar assembly.

Although apoptosis of meiotic cells appears to be one cause of the reduced sperm count in *Ift88*$^{-/-}$, the reduction in sperm count is greater than can be accounted for by the loss of meiotic cells, so other mechanisms must be active. Indeed, sperm cells appear to be lost via phagocytosis by Sertoli cells. Normally at stage IX, mature wild-type sperm have been released into the lumen, and elongated condensed heads are not visible. At this stage, the next generation of spermatids is at step 9 and just beginning to undergo nuclear condensation and elongation (Figure 8E). In contrast to wild type, *Ift88*$^{-/-}$ tubules at stage IX contain numerous highly condensed nuclei in the seminiferous epithelium (Figure 8F). In many cases, these are deep in the epithelium, below the level of the step 9 spermatids (bracket, Figure 8F). It is likely that these represent later-step spermatids that were resorbed by the Sertoli cells during a preceding stage, preventing their release into the lumen.

DISCUSSION

Reduced IFT88 impairs mouse sperm flagellar assembly

The results of this study show that IFT88 is necessary for mammalian spermiogenesis and male fertility. This is in marked contrast to *Drosophila*, for which mutation of either *Ift88* (Han *et al.*, 2003) or a subunit of the IFT motor kinesin-2 (Sarpal *et al.*, 2003) had no effect on sperm formation or male fertility. *Drosophila* sperm axoneme development occurs within the cytoplasm, and the axoneme is not fully enclosed by a flagellar membrane until it is fully elongated (Han *et al.*, 2003). Thus it has been suggested that the axoneme is readily accessible to axonemal precursors in the cytoplasm and IFT is not needed (Han *et al.*, 2003). However, this may not be completely correct, as the tip of the growing axoneme in *Drosophila* is tightly surrounded by an involution of the plasma membrane (Tokuyasu *et al.*, 1972; Gottardo *et al.*, 2013; see Figure 2B in Witman, 2003). This geometry is very similar to the early stages of *Chlamydomonas* flagellar growth, which cannot occur in the absence of IFT88 (Pazour *et al.*, 2000). Therefore *Drosophila* may have evolved an alternative mechanism for delivering axonemal precursors to the membrane-enclosed tip of the elongating axoneme, perhaps to meet novel requirements posed by the assembly of an extremely long (1.8–2.0 mm) flagellum (Han *et al.*, 2003). One possibility is that mRNAs encoding tubulin and other axonemal proteins are present and

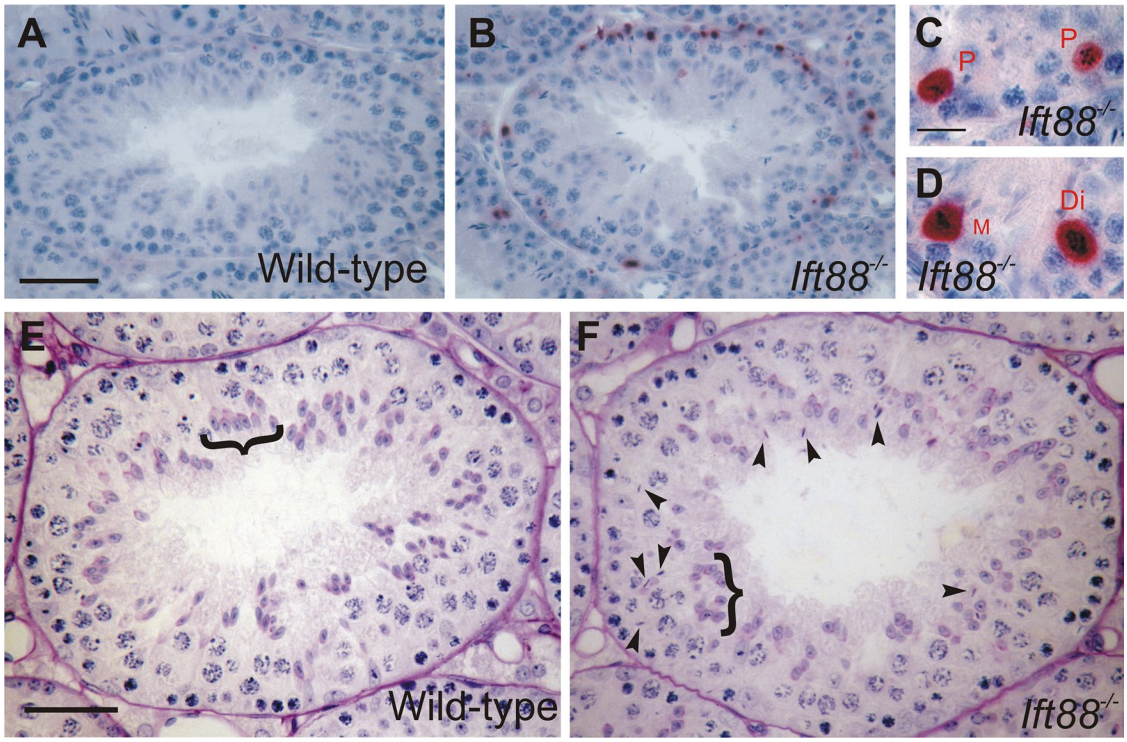

FIGURE 8: Many *Ift88*$^{-/-}$ spermatocytes and spermatids are eliminated by resorption or apoptosis. (A, B) Sections of wild-type (A) and *Ift88*$^{-/-}$ (B) stage IX seminiferous tubules stained by the TUNEL procedure to reveal apoptotic and/or necrotic cells. No apoptotic cells were observed in the wild-type tubule, but numerous TUNEL-positive cells were present in the *Ift88*$^{-/-}$ tubule. The sections were counterstained with hematoxylin. (C, D) Higher-magnification images of *Ift88*$^{-/-}$ tubules in stages IX (C) and XI (D) revealed TUNEL-positive cells that appeared to have reached the pachytene (P), diplotene (Di), and metaphase (M) stages. (E) Cross-section of a wild-type stage IX seminiferous tubule. The mature spermatids have been released, so no condensed nuclei are visible in the seminiferous epithelium. The next generation of spermatids (bracket) is at step 9 and is nearing the tubule lumen. PAS-hematoxylin staining. (F) A comparable section through an *Ift88*$^{-/-}$ stage IX seminiferous tubule. Numerous elongated heads with condensed nuclei (arrowheads) are visible deep in the seminiferous epithelium, many even below the level of the step 9 spermatids (bracket) present at this stage, suggesting that the elongated spermatids have been resorbed by the Sertoli cells. PAS-hematoxylin staining. Scale, bars, 20 μm (A, B, E, F), 5 μm (C, D).

translated within the membrane cap surrounding the tip of the axoneme (Fabian and Brill, 2012), ensuring that the axonemal precursors are continuously available without the need for transport over great distances. In contrast, in the mouse, ribosomes are abundant in the spermatid caudal cytoplasm, including around the developing midpiece, but we never observed ribosomes in the developing flagellum distal to the annulus.

Assembly of flagellar axoneme and accessory structures in *Ift88*$^{-/-}$ spermatids

In *Chlamydomonas*, axonemal components, including tubulin, inner and outer arm dynein, nexin–dynein regulatory complex subunits, and radial spokes, are transported to the tip of the flagellum by IFT (Piperno *et al.*, 1996; Hou *et al.*, 2007; Wren *et al.*, 2013; Craft *et al.*, 2015). Mouse sperm flagella contain all of these components but also contain fibrous sheath and outer dense fiber accessory structures, which are aberrant in the *Ift88*$^{-/-}$ mouse. This is particularly apparent for the fibrous sheath. The fibrous sheath is composed of proteins organized into two longitudinal columns that run along the axoneme and are connected by semicircular ribs. The longitudinal columns normally assemble in a distal-to-proximal direction soon after formation of the full-length axoneme (Irons and Clermont, 1982), but they are never observed in the *Ift88*$^{-/-}$ flagellum. The failure to assemble may be because the mutant flagella do not become sufficiently long to initiate assembly or because longitudinal column proteins are not moved into the mutant flagellum. In contrast to the lack of longitudinal columns, the *Ift88*$^{-/-}$ flagella contain large accumulations of fibrous sheath rib material in their swollen tips. This accumulation strongly suggests that the rib material is actively transported to the flagellar tip. It may be carried by a non-IFT mechanism; if it is carried by IFT, it is not dependent upon wild-type levels of IFT88.

In the *Ift88*$^{-/-}$ spermatids, outer dense fibers assemble ectopically in the caudal cytoplasm when there is no midpiece axoneme to organize them. In these cases, the mitochondria condense around single or small groups of outer dense fibers, demonstrating that the outer dense fibers alone are sufficient to organize the mitochondrial sheath. In flagella of the mutant, outer dense fiber material appears to be in excess of assembled axonemal proteins, causing ectopic outer dense fibers to form on singlet or doublet microtubules where no axoneme is present. These observations indicate that outer dense fibers have a strong affinity for microtubules but that an intact axoneme is required to organize them into a ninefold array. Because outer dense fibers assemble from base to tip and are present in *Ift88*$^{-/-}$ sperm flagella, their precursors also are likely to be transported to their site of assembly by a mechanism not dependent on

normal levels of IFT88. Lehti *et al.* (2013) reported that the outer dense fiber protein ODF3 was coimmunoprecipitated with KIF3A, raising the possibility that it is coupled directly to kinesin-2 for import into the developing flagellum.

The presence of many unorganized singlet and doublet microtubules in the *Ift88*$^{-/-}$ flagella indicates that tubulin also has been transported into the flagellum in considerable excess of what has assembled into 9 + 2 axonemes. Assuming that IFT-B lacking IFT88 is trafficked through flagella, this is consistent with the prediction of Bhogaraju *et al.* (2013) that two other IFT-B proteins, IFT81 and IFT74, together form a tubulin-binding module for transport of tubulin by IFT. The fact that the microtubules in the *Ift88*$^{-/-}$ flagellum often are not organized into an axoneme probably is due to a failure of IFT to deliver minor proteins that are essential for assembly of the axonemal superstructure.

IFT88 normally is expressed before the time when abnormalities appear in mutant germ cells

The synthesis of IFT88 protein was first detected in early pachytene spermatocytes, and the protein was highly expressed in midpachytene spermatocytes, well before flagellar assembly or nuclear reshaping is initiated after meiosis. Because there is no evidence that IFT88 participates in meiosis, it is probable that the germ cell makes IFT88 at this time so that there will be an ample pool available when flagellar growth is initiated shortly after meiosis. This timing of expression is only slightly earlier than that of the cAMP-dependent protein kinase catalytic subunit Cα_2, which is a component of the axoneme (San Agustin and Witman, 2001) and is first expressed in midpachytene spermatocytes (San Agustin *et al.*, 2000). It also is consistent with a report that synthesis of SDS-soluble sperm proteins is highest during meiosis (O'Brien and Bellve, 1980). Of interest, expression of KIF3A also was first detected in pachytene spermatocytes and subsequently increased (Lehti *et al.*, 2013). The timing of expression of IFT88 is in contrast to that of the accessory structure proteins ropporin and Odf2, which were first detected in step 4 and 12 postmeiotic spermatids, respectively. These proteins are incorporated into the flagellum only after its elongation has been completed, so presumably there is no need to accumulate a pool of them before flagellar assembly.

Apoptosis was observed in *Ift88*$^{-/-}$ spermatocytes that had reached the late pachytene, diplotene, and metaphase stages. This is before flagellar assembly or nuclear reshaping, so defects in these processes cannot have been the cause of apoptosis in these cells. Because large amounts of IFT88 protein normally are made before or during these stages, it is likely that spermatocytes have a highly sensitive mechanism to detect the amount of IFT88 that has accumulated and respond by programmed cell death when the levels are insufficient for subsequent spermatogenic processes. If such a monitoring mechanism extends to sperm structural proteins, it might explain the absence of mature flagellated sperm in other mouse models with defects in minor axonemal structures that do not preclude assembly of tracheal cilia and are not necessary for assembly of *Chlamydomonas* flagella (Lee *et al.*, 2008; DiPetrillo and Smith, 2010; Brown *et al.*, 2012; McKenzie *et al.*, 2015). Another possibility is that IFT88 has a role in some spermatogenic process preceding nuclear reshaping and flagellar assembly.

IFT is not present in mature sperm

With the exception of the *Drosophila* sperm flagella discussed earlier and *Plasmodium*, which is ciliated but lacks IFT genes (van Dam *et al.*, 2013), IFT has been found in all cilia and flagella examined (Rosenbaum and Witman, 2002). Moreover, IFT has been visualized in full-length flagella of *Chlamydomonas* (Kozminski *et al.*, 1993) and *Trypanosoma* (Buisson *et al.*, 2013), in mature sensory cilia of *C. elegans* (Signor *et al.*, 1999), in motile epidermal cilia of X*enopus* multiciliated cells (Brooks and Wallingford, 2012), and in fully formed primary cilia in cultured mammalian cells (Follit *et al.*, 2006; Tran *et al.*, 2008; Ishikawa and Marshall, 2015), indicating that it continues to have a function in most cilia and flagella, including those of terminally differentiated cells, after their assembly. When *Chlamydomonas* strains with temperature-sensitive mutations in the anterograde or retrograde IFT motors are allowed to form full-length flagella at permissive temperature and then shifted to restrictive temperatures, the flagella shorten, indicating that IFT is necessary for continued maintenance of flagellar length (Kozminski *et al.*, 1993; Engel *et al.*, 2012; Witman, 2012). This undoubtedly reflects a need for IFT to replace axonemal components that undergo turnover at the flagellar tip (Marshall and Rosenbaum, 2001) and to move the products of this turnover out of the flagellum. IFT also functions in moving proteins, including signaling proteins, between the mature cilium or flagellum and the cell body (Pan and Snell, 2003; Goetz and Anderson, 2010; Liem *et al.*, 2012; Eguether *et al.*, 2014) and in the turnover of membrane components, including receptors (Pazour and Witman, 2003; Lechtreck *et al.*, 2009, 2013). Therefore it is notable that none of the IFT components that we have examined are present in the mature mammalian sperm. The mammalian sperm differs from most other ciliated and flagellated cells in that it has virtually no cytoplasm, no protein synthesis, and presumably no pool of flagellar precursors, so it is highly improbable that it undergoes turnover of flagellar components. Moreover, although signals may move from the head to the tail and vice versa, these signals are likely to be mediated by ions or small molecules rather than IFT (Kirichok *et al.*, 2006). Therefore the mature mammalian sperm lacks processes mediated by IFT in other cilia and flagella and, in the absence of these processes, has dispensed with the IFT system.

MATERIALS AND METHODS

Mouse breeding

Mice used for this work were a recombinant inbred line derived from C3H/HeJ and FvB/NJ containing the wild-type *Pde6b* (*Rd1*) allele from C57BL/6J and the *Ift88*^{Tg737Rpw} mutation (Moyer *et al.*, 1994). Mutant (*Ift88*$^{-/-}$) and control (*Ift88*$^{+/+}$ or *Ift88*$^{+/-}$) animals were derived from heterozygous-by-heterozygous crosses (Pazour *et al.*, 2000, 2002).

For fertility testing, five control and five *Ift88*$^{-/-}$ males were each paired with two wild-type C57BL/6J females. Plug formation was checked daily during the first week, and litters were tracked for the duration of the study. After 6 wk, the females were separated from the males for 3 wk to ensure that paternity could be established. After this 3-wk period, the males were swapped so that females exposed to mutant males were paired with control males and vice versa. The second mating phase was terminated after 6 wk.

All mouse work was performed with approval of the University of Massachusetts Medical School Institutional Animal Care and Use Committee.

Antibodies and reagents

Rabbit antibodies against mouse IFT140, IFT88, IFT57, and IFT20 were made and affinity purified as described (Pazour *et al.*, 2002; Jonassen *et al.*, 2012). Affinity-purified rabbit anti-ropporin (Fujita *et al.*, 2000) was a gift from Shuh Narumiya (Department of Pharmacology, Kyoto University Faculty of Medicine, Kyoto, Japan). Affinity-purified rabbit anti-Odf2 (Hoyer-Fender *et al.*, 1995) was a gift

from Sigrid Hoyer-Fender (Department of Zoology-Developmental Biology, University of Göttingen, Göttingen, Germany). The affinity-purified anti-Cα_2 antibody was described previously (San Agustin *et al.*, 2000). Monoclonal anti–α-tubulin antibody (clone B-5-1-2) and monoclonal anti–acetylated α-tubulin antibody 6-11B-1 were purchased from Sigma-Aldrich (St. Louis, MO).

Northern and Western blotting

Northern blotting was performed according to standard procedures (Sambrook *et al.*, 1987) using a Mouse Multiple Tissue Northern Blot (7762-1, BD Biosciences, Palo Alto, CA) and random-primed, ^{32}P-labeled cDNA as a probe. Testis extracts and Western blots were prepared as described previously (San Agustin *et al.*, 2000; San Agustin and Witman, 2001). Some used Western blots were stripped by overnight incubation at room temperature with Restore Western Blot Stripping Buffer (Pierce Biotechnology, Rockford, IL), treated with blocker and then reprobed with a different antibody.

Sucrose gradient fractionation of testis extracts

Two testes were excised, placed in 500 µl of ice-cold extraction buffer (35 mM $NaHCO_3$, 2 mM Na_2HPO_4, 70 mM KCl, 74 mM NaCl [McGrady, 1979], 1 mM dithiothreitol, 0.16% digitonin, 10 mM 4-aminobenzamidine, 2 mM EDTA, 50 µM leupeptin, 15 µM pepstatin, 200 µM tosyl phenylalanyl chloromethyl ketone, 100 µM tosyl lysine chloromethyl ketone, 1 µg/ml aprotinin, final pH 7.4) and homogenized in a Potter-Elvehjem tissue grinder. The homogenate was centrifuged at 6500 × *g* for 15 min at 4°C and further clarified at 56,000 × *g* for 1 h at 4°C. The clarified testis extract was layered on a 5–20% sucrose gradient that had the same buffer composition as the extraction buffer minus digitonin, and centrifuged at 4°C in a Beckman L5-75 ultracentrifuge (36,000 rpm, SW41 rotor). The cumulative centrifugal effect ($\omega^2 t$) for all runs was set at 6.4×10^{10} rad^2/s. Sedimentation standards were thyroglobulin (19.4S), catalase (11.3S), and bovine serum albumin (BSA; 4.4S; Cole *et al.*, 1998). Sucrose gradient fractions (500 µl) were collected, and the proteins were separated by SDS–PAGE, transferred to polyvinylidene fluoride membranes, and probed with anti-IFT antibodies.

Examination and counting of epididymal sperm

Cauda epididymides were excised and cleared of fatty tissue. The vas deferens was cut, with a short portion left to serve as outlet for the sperm. The sperm were then prodded out of the epididymis with a blunt 21-gauge needle into 1 ml of PBS and counted using a hemocytometer. For morphological examination by differential interference contrast microscopy, the extruded sperm were collected by centrifugation (2000 rpm, 5 min, IEC Micromax), suspended in PBS to 2×10^7/ml, and mixed with an equal volume of 2× fixing solution (4% formaldehyde in 100 mM sodium phosphate, pH 7.4; 2 h at 4°C). About 50 µl of the fixed sperm was placed on a coverslip coated with 0.1% polyethyleneimine (Sigma-Aldrich), allowed to settle for 10 min, and then blotted off. The coverslip was washed three times with PBS and then mounted with Glycergel (Dako, Carpinteria, CA).

Histology of mouse testis

Fixation of testes. Bouin's fixative was introduced by vascular perfusion through the heart (Sprando, 1990). The mouse was given an intraperitoneal injection of heparin (Sigma-Aldrich) at 130 IU/kg body weight and then anesthetized with isoflurane 15 min later. The left ventricle was punctured with a blunted 22-gauge needle attached to a saline reservoir 3 ft above the animal. The right ventricle was cut immediately to allow a constant outflow of perfusate. After the perfusate had cleared of blood (~5 min), the fixative was switched on and allowed to perfuse through the mouse for 30 min. The testes were then removed and each one cut into two longitudinal sections and further exposed overnight to the fixative at 4°C. After several 30-min washes with PBS, the testes were washed with 50% ethanol to remove residual picric acid.

Immunohistochemistry. The fixed testes were embedded in paraffin for immunohistochemistry or LR White (Electron Microscopy Sciences, Fort Washington, PA) for histological studies. The procedure for antibody labeling was as described previously (San Agustin *et al.*, 2000) with the following modifications. Antigens were retrieved by microwave heating (Panasonic model NN-5408A at high setting) for 10 min in 10 mM sodium citrate, pH 6. Before blocking with normal swine serum (Dako), the sections were treated with a biotin blocking system (Dako), which eliminated the faint background staining in the interstitial cells. For detection of IFT88, ropporin, and Odf2, sections were incubated overnight at 4°C with anti-IFT88 (1:200), anti-ropporin (1:250), or anti-Odf2 (1:250). Biotinylated F(ab')2 fragment of affinity-isolated swine anti-rabbit immunoglobulins (Dako) was then applied (diluted to 0.71 µg /ml with TBS, 1% BSA [fraction V, fatty acid-free; Calbiochem/EMD Biosciences, San Diego, CA]), followed by alkaline phosphatase–conjugated streptavidin (diluted to 0.90 µg/ml; Dako). Exposure time was 20 min for both. The sections were washed with TBS between incubations. Labeling was visualized using the BCIP/NBT/INT substrate system (Dako), with a reaction time of 20–30 min. The sections were counterstained with hematoxylin (5 min), cleared with saturated lithium carbonate (1 min), and mounted with Glycergel.

Periodic acid-Schiff staining. The solutions used in PAS staining were prepared according to Tran *et al.* (2008). LR White sections (3 µm) were immersed in periodic acid for 1 h. After a brief rinse with water, they were transferred to the Schiff reagent for 1 h, rinsed with three changes (10 min each) of the sulfite solution, washed in running water (30 min), counterstained with hematoxylin (20 min), cleared with saturated lithium carbonate (2 min), air dried, and mounted with Shandon mount (Shandon, Pittsburgh, PA).

Electron microscopy. Testes were fixed by vascular perfusion as described, except that 5% glutaraldehyde in 50 mM sodium cacodylate, pH 7.4, was used as fixative. After perfusion, the testes were diced into 1-mm cubes, fixed in glutaraldehyde for another hour, washed with cacodylate buffer at 4°C, and then postfixed with 1% osmium tetroxide in 50 mM sodium cacodylate buffer, pH 7.4, at room temperature for 1 h. The tissue pieces were then washed three times in fresh cacodylate buffer and stained overnight at 4°C with fresh 1% uranyl acetate. After washing with water, the tissues were dehydrated through a graded series of ethanol and transferred to propylene oxide and finally into a 50:50 (vol/vol) mixture of Embed 812 (Electron Microscopy Sciences, Hatfield, PA) and propylene oxide for overnight infiltration. They were then transferred through three changes of fresh resin (1 h each) and finally polymerized at 60°C for 48 h.

Isolation of spermatogenic cells. All containers used were either siliconized or made of polypropylene. The two testes of an adult male (at least 8 wk old) were excised, transferred to 5 ml of KRB complete in a small Petri dish, and decapsulated. KRB complete is made up of Krebs–Ringer bicarbonate buffer (Sigma-Aldrich) plus 1.3 mM $CaCl_2$, 1 mM glutamine, and 10 ml/l each of essential and nonessential amino acids (GIBCO/Invitrogen, Grand Island, NY), pH 6.9. The testes were then placed in 10 ml of 1 mg/ml collagenase

A (Roche Applied Science, Indianapolis, IN) in KRB complete and incubated at 34°C for 15 min in a shaking water bath to uncoil the seminiferous tubules. The uncoiled tubules were allowed to settle, and the supernatant (which contained interstitial cells) was discarded. The tubules were washed three times (10 ml each) with KRB complete and resuspended in 5 ml of KRB complete. They were then diced (Vannas scissors; Ted Pella, Redding, CA) and aspirated from time to time to release the spermatogenic cells. The cell suspension was allowed to settle for 1 min, the supernatant collected, and the process repeated. The two supernatants (~10 ml) were pooled and centrifuged (1000 rpm, 10 min, RC-5B centrifuge, SS-34 rotor) to collect the cells.

The soft pellet of cells obtained was resuspended in 1 ml of KRB complete and gently aspirated. The suspension was then layered on top of a Percoll step gradient (15, 22, 30, 45, and 90%, 1 ml each) and centrifuged at 2500 rpm for 30 min (RC-5B centrifuge, SS-34 rotor). The Percoll solutions were made by diluting Percoll in KRB basic (KRB complete minus $CaCl_2$, glutamine, and essential and nonessential amino acids). The spermatogenic cells usually collected between the 30 and 45% Percoll layers and were then resuspended in KRB basic to the desired density.

Fixation of spermatogenic cells. An equal volume of 2× fixing solution (4% paraformaldehyde in PBS) was added to the cell suspension and the cells fixed for ~5 h on ice with constant, gentle shaking. An equal volume of 2% paraformaldehyde and 0.2% Triton X-100 in PBS was then added and the incubation continued for 30 min to permeabilize and further fix the cells. About 100 µl of fixed, permeabilized cells was then pipetted onto coverslips coated with 0.1% polyethyleneimine, allowed to settle for 10 min, and washed three times with 250 µl of PBS. The coverslips were stored in 400 µl of PBS at 4°C.

Immunofluorescence microscopy. Coverslips containing the fixed spermatogenic cells were rinsed with TBS and endogenous biotin blocked (Dako) following manufacturer's instructions. This was followed by 1-h incubation in a blocking buffer (Tris-buffered saline [TBS], 5% BSA fatty-acid free, 10% nonimmune goat serum). Overnight double antibody labeling at 4°C was performed using 1) a polyclonal rabbit antibody to IFT88 and 2) a mouse monoclonal anti–α-tubulin antibody as marker for microtubules, including those of the manchette and axoneme. The latter was prepared by first incubating at room temperature the monoclonal anti–α-tubulin antibody (1:1000) with the F(ab')2 fragments of a goat anti-mouse immunoglobulin G (IgG) conjugated to Alexa 568 in TBS plus 1% BSA for 2 h, followed by 1-h incubation with normal mouse serum at 10% final concentration (to saturate the binding sites of the goat anti-mouse IgG F(ab')2 fragments). The rabbit anti-IFT88 antibody was added to this mixture just before use. On the next day the coverslips were rinsed three times in 250 µl of 1/5 blocking buffer. They were then incubated for 20 min with a 1:800 dilution of biotin-conjugated F(ab')2 fragment of goat anti-rabbit IgG in TBS and 1% BSA, rinsed three times with 250 µl of 1/5 blocking buffer, and then incubated for 20 min with a 1:400 dilution of streptavidin-conjugated Alexa Fluor 488 in TBS plus 0.5% BSA. After rinsing three times in TBS, the coverslips were counterstained with 0.5 µM TOTO-3 in TBS for 5 min, rinsed three times with TBS, and mounted using Prolong antifade. The fluorescent antibody and streptavidin conjugates, TOTO-3, and Prolong antifade were all purchased from Molecular Probes/Invitrogen (Eugene, OR).

Epididymal sperm were collected and fixed as described. After the 2-h fixation, they were permeabilized by mixing with an equal volume of fixative containing 0.1% SDS and left on ice for 15 min. About 200 µl of the permeabilized sperm was placed on a Superfrost Plus microscope slide (Fisher Scientific, Waltham, MA) and allowed to settle for 10 min. Slides were then washed with PBS, blocked with 1% BSA in TBS/Tween (TBST), and incubated with anti–acetylated α-tubulin antibody 6-11B-1 and anti-IFT88 antibody overnight at 4°C. Labeling by 6-11B-1 was visualized with Alexa Fluor 568 secondary antibody to mouse IgG; anti-IFT88 labeling was visualized with Alexa Fluor 488 secondary antibody to rabbit IgG (both secondary antibodies from Life Technologies, Carlsbad, CA). Between antibody incubations, slides were washed with 1% BSA in TBST. Nuclei were stained with 4′,6-diamidino-2-phenylindole dihydrochloride (DAPI; Invitrogen). Slides were mounted with coverslips using Prolong Gold Antifade (Life Technologies).

Counting of germ-cell population in seminiferous tubule cross-sections

The procedure described by Oakberg (1956) was followed. Measurements were performed on 3-µm-thick LR White sections stained with PAS and hematoxylin. A crude value for the population of a particular germ cell in the tubule cross-section was obtained by counting all of their visible nuclei. The final, corrected count was obtained using the formula $F = C[t/(t + d)]$, where F is the final count, C is the crude count, t is the section thickness, and d is the nuclear diameter. Nuclear diameters were measured using an ocular micrometer and then averaged.

Detection of apoptotic cells

Testes were fixed with Bouin's fixative as described and embedded in paraffin. Cut sections, typically 6 µm thick, were dewaxed in toluene and rehydrated with a graded series of isopropanol. The sections were transferred to 500 ml of 10 mM sodium citrate, pH 6, and heated for 5 min in a microwave oven (high setting). This partially disrupts the formaldehyde cross-links formed during the fixation process, thereby permeabilizing the sections. The permeabilized sections were cooled to room temperature with running tap water and then analyzed for apoptotic cells using the In Situ Cell Death Detection Kit, AP (Roche Molecular Biochemicals, Indianapolis, IN). The protocol recommended in the kit was followed, except that permeabilization was accomplished as described. The TdT enzyme stock solution was diluted 1:5 with the TUNEL dilution buffer (30 mM Tris-HCl, 140 mM sodium cacodylate, 1 mM $CoCl_2$, pH 6.6). The kit used fluorescein-labeled nucleotides as substrates for the TUNEL reaction. The sections were blocked (TBS containing 5% BSA, 20% normal rabbit serum) and the fluorescein-tagged, newly synthesized DNA products in apoptotic cells were then reacted with alkaline phosphatase–conjugated anti-fluorescein antibody. Antibody binding was visualized using a fuchsin substrate system (Dako). Color (magenta) was allowed to develop for 10 min, after which the sections were rinsed in water, counterstained with hematoxylin (5 min), cleared with saturated lithium carbonate solution (1 min), and mounted with Glycergel.

ACKNOWLEDGMENTS

We are grateful to Shuh Narumiya and Sigrid Hoyer-Fender for antibodies. We thank Paul Odgren (University of Massachusetts Medical School) for use of his bright-field microscope and Gregory Hendricks (Electron Microscopy Core, University of Massachusetts Medical School) for assistance with electron microscopy. This work was supported by National Institutes of Health Grants GM60992 (G.J.P.) and GM30626 (G.B.W.), the Bushrod H. Campbell and Adah F. Hall Charity Fund (G.W.), and the Robert W. Booth Fund at the University of Massachusetts Medical School (G.W.).

REFERENCES

Absalon S, Blisnick T, Kohl L, Toutirais G, Dore G, Julkowska D, Tavenet A, Bastin P (2008). Intraflagellar transport and functional analysis of genes required for flagellum formation in trypanosomes. Mol Biol Cell 19, 929–944.

Avidor-Reiss T, Maer AM, Koundakjian E, Polyanovsky A, Keil T, Subramaniam S, Zuker CS (2004). Decoding cilia function: defining specialized genes required for compartmentalized cilia biogenesis. Cell 117, 527–539.

Bangs FK, Schrode N, Hadjantonakis AK, Anderson KV (2015). Lineage specificity of primary cilia in the mouse embryo. Nat Cell Biol 17, 113–122.

Banizs B, Pike MM, Millican CL, Ferguson WB, Komlosi P, Sheetz J, Bell PD, Schwiebert EM, Yoder BK (2005). Dysfunctional cilia lead to altered ependyma and choroid plexus function, and result in the formation of hydrocephalus. Development 132, 5329–5339.

Bhogaraju S, Cajanek L, Fort C, Blisnick T, Weber K, Taschner M, Mizuno N, Lamla S, Bastin P, Nigg EA, Lorentzen E (2013). Molecular basis of tubulin transport within the cilium by IFT74 and IFT81. Science 341, 1009–1012.

Boehlke C, Kotsis F, Buchholz B, Powelske C, Eckardt KU, Walz G, Nitschke R, Kuehn EW (2013). Kif3a guides microtubular dynamics, migration and lumen formation of MDCK cells. PLoS One 8, e62165.

Brazelton WJ, Amundsen CD, Silflow CD, Lefebvre PA (2001). The bld1 mutation identifies the Chlamydomonas osm-6 homolog as a gene required for flagellar assembly. Curr Biol 11, 1591–1594.

Brooks ER, Wallingford JB (2012). Control of vertebrate intraflagellar transport by the planar cell polarity effector Fuz. J Cell Biol 198, 37–45.

Brown JM, DiPetrillo CG, Smith EF, Witman GB (2012). A FAP46 mutant provides new insights into the function and assembly of the C1d complex of the ciliary central apparatus. J Cell Sci 125, 3904–3913.

Brown JM, Marsala C, Kosoy R, Gaertig J (1999). Kinesin-II is preferentially targeted to assembling cilia and is required for ciliogenesis and normal cytokinesis in *Tetrahymena*. Mol Biol Cell 10, 3081–3096.

Buisson J, Chenouard N, Lagache T, Blisnick T, Olivo-Marin JC, Bastin P (2013). Intraflagellar transport proteins cycle between the flagellum and its base. J Cell Sci 126, 327–338.

Cano DA, Murcia NS, Pazour GJ, Hebrok M (2004). *orpk* mouse model of polycystic kidney disease reveals essential role of primary cilia in pancreatic tissue organization. Development 131, 3457–3467.

Cole DG, Diener DR, Himelblau AL, Beech PL, Fuster JC, Rosenbaum JL (1998). *Chlamydomonas* kinesin-II-dependent intraflagellar transport (IFT): IFT particles contain proteins required for ciliary assembly in *Caenorhabditis elegans* sensory neurons. J Cell Biol 141, 993–1008.

Collet J, Spike CA, Lundquist EA, Shaw JE, Herman RK (1998). Analysis of *osm*-6, a gene that affects sensory cilium structure and sensory neuron function in *Caenorhabditis elegans*. Genetics 148, 187–200.

Craft JM, Harris JA, Hyman S, Kner P, Lechtreck KF (2015). Tubulin transport by IFT is upregulated during ciliary growth by a cilium-autonomous mechanism. J Cell Biol 208, 223–237.

Davenport JR, Watts AJ, Roper VC, Croyle MJ, van Groen T, Wyss JM, Nagy TR, Kesterson RA, Yoder BK (2007). Disruption of intraflagellar transport in adult mice leads to obesity and slow-onset cystic kidney disease. Curr Biol 17, 1586–1594.

Davidge JA, Chambers E, Dickinson HA, Towers K, Ginger ML, McKean PG, Gull K (2006). Trypanosome IFT mutants provide insight into the motor location for mobility of the flagella connector and flagellar membrane formation. J Cell Sci 119, 3935–3943.

DiPetrillo CG, Smith EF (2010). Pcdp1 is a central apparatus protein that binds Ca^{2+}-calmodulin and regulates ciliary motility. J Cell Biol 189, 601–612.

Dym M (1994). Spermatogonial stem cells of the testis. Proc Natl Acad Sci USA 91, 11287–11289.

Eguether T, San Agustin JT, Keady BT, Jonassen JA, Liang Y, Francis R, Tobita K, Johnson CA, Abdelhamed ZA, Lo CW, Pazour GJ (2014). IFT27 links the BBSome to IFT for maintenance of the ciliary signaling compartment. Dev Cell 31, 279–290.

Engel BD, Ishikawa H, Wemmer KA, Geimer S, Wakabayashi K, Hirono M, Craige B, Pazour GJ, Witman GB, Kamiya R, Marshall WF (2012). The role of retrograde intraflagellar transport in flagellar assembly, maintenance, and function. J Cell Biol 199, 151–167.

Fabian L, Brill JA (2012). Drosophila spermiogenesis: big things come from little packages. Spermatogenesis 2, 197–212.

Follit JA, Tuft RA, Fogarty KE, Pazour GJ (2006). The intraflagellar transport protein IFT20 is associated with the Golgi complex and is required for cilia assembly. Mol Biol Cell 17, 3781–3792.

Follit JA, Xu F, Keady BT, Pazour GJ (2009). Characterization of mouse IFT complex B. Cell Motil Cytoskeleton 66, 457–468.

Fujita A, Nakamura K, Kato T, Watanabe N, Ishizaki T, Kimura K, Mizoguchi A, Narumiya S (2000). Ropporin, a sperm-specific binding protein of rhophilin, that is localized in the fibrous sheath of sperm flagella. J Cell Sci 113, 103–112.

Gilley SK, Stenbit AE, Pasek RC, Sas KM, Steele SL, Amria M, Bunni MA, Estell KP, Schwiebert LM, Flume P, *et al*. (2014). Deletion of airway cilia results in noninflammatory bronchiectasis and hyperreactive airways. Am J Physiol Lung Cell Mol Physiol 306, L162–L169.

Goetz SC, Anderson KV (2010). The primary cilium: a signalling centre during vertebrate development. Nat Rev Genet 11, 331–344.

Gottardo M, Callaini G, Riparbelli MG (2013). The cilium-like region of the *Drosophila* spermatocyte: an emerging flagellum? J Cell Sci 126, 5441–5452.

Guan J, Kinoshita M, Yuan L (2009). Spatiotemporal association of DNAJB13 with the annulus during mouse sperm flagellum development. BMC Dev Biol 9, 23.

Han YG, Kwok BH, Kernan MJ (2003). Intraflagellar transport is required in *Drosophila* to differentiate sensory cilia but not sperm. Curr Biol 13, 1679–1686.

Hou Y, Qin H, Follit JA, Pazour GJ, Rosenbaum JL, Witman GB (2007). Functional analysis of an individual IFT protein: IFT46 is required for transport of outer dynein arms into flagella. J Cell Biol 176, 653–665.

Hoyer-Fender S, Burfeind P, Hameister H (1995). Sequence of mouse Odf1 cDNA and its chromosomal localization: extension of the linkage group between human chromosome 8 and mouse chromosome 15. Cytogenet Cell Genet 70, 200–204.

Hoyer-Fender S, Petersen C, Brohmann H, Rhee K, Wolgemuth DJ (1998). Mouse Odf2 cDNAs consist of evolutionary conserved as well as highly variable sequences and encode outer dense fiber proteins of the sperm tail. Mol Reprod Dev 51, 167–175.

Irons MJ, Clermont Y (1982). Kinetics of fibrous sheath formation in the rat spermatid. Am J Anat 165, 121–130.

Ishikawa H, Marshall WF (2015). Efficient live fluorescence imaging of intraflagellar transport in mammalian primary cilia. Methods Cell Biol 127, 189–201.

Jonassen JA, SanAgustin J, Baker SP, Pazour GJ (2012). Disruption of IFT complex A causes cystic kidneys without mitotic spindle misorientation. J Am Soc Nephrol 23, 641–651.

Keady BT, Le YZ, Pazour GJ (2011). IFT20 is required for opsin trafficking and photoreceptor outer segment development. Mol Biol Cell 22, 921–930.

Keady BT, Samtani R, Tobita K, Tsuchya M, San Agustin JT, Follit JA, Jonassen JA, Subramanian R, Lo CW, Pazour GJ (2012). IFT25 links the signal-dependent movement of Hedgehog components to intraflagellar transport. Dev Cell 22, 940–951.

Kierszenbaum AL, Rivkin E, Tres LL, Yoder BK, Haycraft CJ, Bornens M, Rios RM (2011). GMAP210 and IFT88 are present in the spermatid golgi apparatus and participate in the development of the acrosome-acroplaxome complex, head-tail coupling apparatus and tail. Dev Dyn 240, 723–736.

Kirichok Y, Navarro B, Clapham DE (2006). Whole-cell patch-clamp measurements of spermatozoa reveal an alkaline-activated Ca^{2+} channel. Nature 439, 737–740.

Kozminski KG, Beech PL, Rosenbaum JL (1995). The *Chlamydomonas* kinesin-like protein FLA10 is involved in motility associated with the flagellar membrane. J Cell Biol 131, 1517–1527.

Kozminski KG, Johnson KA, Forscher P, Rosenbaum JL (1993). A motility in the eukaryotic flagellum unrelated to flagellar beating. Proc Natl Acad Sci USA 90, 5519–5523.

Kramer-Zucker AG, Olale F, Haycraft CJ, Yoder BK, Schier AF, Drummond IA (2005). Cilia-driven fluid flow in the zebrafish pronephros, brain and Kupffer's vesicle is required for normal organogenesis. Development 132, 1907–1921.

Kwitny S, Klaus AV, Hunnicutt GR (2010). The annulus of the mouse sperm tail is required to establish a membrane diffusion barrier that is engaged during the late steps of spermiogenesis. Biol Reprod 82, 669–678.

Leblond CP, Clermont Y (1952). Definition of the stages of the cycle of the seminiferous epithelium in the rat. Ann NY Acad Sci 55, 548–573.

Lechtreck KF, Brown JM, Sampaio JL, Craft JM, Shevchenko A, Evans JE, Witman GB (2013). Cycling of the signaling protein phospholipase D through cilia requires the BBSome only for the export phase. J Cell Biol 201, 249–261.

Lechtreck KF, Johnson EC, Sakai T, Cochran D, Ballif BA, Rush J, Pazour GJ, Ikebe M, Witman GB (2009). The *Chlamydomonas reinhardtii* BBSome is an IFT cargo required for export of specific signaling proteins from flagella. J Cell Biol 187, 1117–1132.

Lee L, Campagna DR, Pinkus JL, Mulhern H, Wyatt TA, Sisson JH, Pavlik JA, Pinkus GS, Fleming MD (2008). Primary ciliary dyskinesia in mice lacking the novel ciliary protein Pcdp1. Mol Cell Biol 28, 949–957.

Lehman JM, Laag E, Michaud EJ, Yoder BK (2009). An essential role for dermal primary cilia in hair follicle morphogenesis. J Invest Dermatol 129, 438–448.

Lehti MS, Kotaja N, Sironen A (2013). KIF3A is essential for sperm tail formation and manchette function. Mol Cell Endocrinol 377, 44–55.

Liem KF Jr, Ashe A, He M, Satir P, Moran J, Beier D, Wicking C, Anderson KV (2012). The IFT-A complex regulates Shh signaling through cilia structure and membrane protein trafficking. J Cell Biol 197, 789–800.

Marshall WF, Rosenbaum JL (2001). Intraflagellar transport balances continuous turnover of outer doublet microtubules: implications for flagellar length control. J Cell Biol 155, 405–414.

Marszalek JR, Liu X, Roberts EA, Chui D, Marth JD, Williams DS, Goldstein LSB (2000). Genetic evidence for selective transport of opsin and arrestin by kinesin-II in mammalian photoreceptors. Cell 102, 175–187.

Marszalek JR, Ruiz-Lozano P, Roberts E, Chien KR, Goldstein LSB (1999). Situs inversus and embryonic ciliary morphogenesis defects in mouse mutants lacking the KIF3A subunit of kinesin-II. Proc Natl Acad Sci USA 96, 5043–5048.

McDermott KM, Liu BY, Tlsty TD, Pazour GJ (2010). Primary cilia regulate branching morphogenesis during mammary gland development. Curr Biol 20, 731–737.

McGrady A (1979). Electrophysiology of differentiating mouse spermatozoa. J Cell Physiol 99, 223–232.

McKenzie CW, Craige B, Kroeger TV, Finn R, Wyatt TA, Sisson JH, Pavlik JA, Strittmatter L, Hendricks GM, Witman GB, Lee L (2015). CFAP54 is required for proper ciliary motility and assembly of the central pair apparatus in mice. Mol Biol Cell 26, 3140–3149.

Morris RL, Scholey JM (1997). Heterotrimeric kinesin-II is required for the assembly of motile 9+2 ciliary axonemes on sea urchin embryos. J Cell Biol 138, 1009–1022.

Moyer JH, Lee-Tischler MJ, Kwon H-Y, Schrick JJ, Avner ED, Sweeney WE, Godfrey VL, Cacheiro NLA, Wilkinson JE, Woychik RP (1994). Candidate gene associated with a mutation causing recessive polycystic kidney disease in mice. Science 264, 1329–1333.

Mukhopadhyay S, Wen X, Chih B, Nelson CD, Lane WS, Scales SJ, Jackson PK (2010). TULP3 bridges the IFT-A complex and membrane phosphoinositides to promote trafficking of G protein-coupled receptors into primary cilia. Genes Dev 24, 2180–2193.

Murcia NS, Richards WG, Yoder BK, Mucenski ML, Dunlap JR, Woychik RP (2000). The *Oak Ridge Polycystic Kidney (orpk)* disease gene is required for left-right axis determination. Development 127, 2347–2355.

Nachury MV, Loktev AV, Zhang Q, Westlake CJ, Peranen J, Merdes A, Slusarski DC, Scheller RH, Bazan JF, Sheffield VC, Jackson PK (2007). A core complex of BBS proteins cooperates with the GTPase Rab8 to promote ciliary membrane biogenesis. Cell 129, 1201–1213.

Nonaka S, Tanaka Y, Okada Y, Takada S, Harada A, Kanai Y, Kido M, Hirokawa N (1998). Randomization of left-right asymmetry due to loss of nodal cilia generating leftward flow of extraembryonic fluid in mice lacking KIF3B motor protein. Cell 95, 829–837.

Oakberg E (1956). A description of spermiogenesis in the mouse and its use in analysis of the cycle of the seminiferous epithelium and germ cell renewal. Am J Anat 99, 391–314.

O'Brien DA, Bellve AR (1980). Protein constituents of the mouse spermatozoon. II. Temporal synthesis during spermatogenesis. Dev Biol 75, 405–418.

O'Donnell L, Nicholls PK, O'Bryan MK, McLachlan RI, Stanton PG (2011). Spermiation: the process of sperm release. Spermatogenesis 1, 14–35.

Ou G, Blacque OE, Snow JJ, Leroux MR, Scholey JM (2005). Functional coordination of intraflagellar transport motors. Nature 436, 583–587.

Pan J, Snell WJ (2003). Kinesin II and regulated intraflagellar transport of *Chlamydomonas* aurora protein kinase. J Cell Sci 116, 2179–2186.

Pazour GJ, Baker SA, Deane JA, Cole DG, Dickert BL, Rosenbaum JL, Witman GB, Besharse JC (2002). The intraflagellar transport protein, IFT88, is essential for vertebrate photoreceptor assembly and maintenance. J Cell Biol 157, 103–113.

Pazour GJ, Dickert BL, Vucica Y, Seeley ES, Rosenbaum JL, Witman GB, Cole DG (2000). *Chlamydomonas IFT*88 and its mouse homologue, polycystic kidney disease gene *Tg737*, are required for assembly of cilia and flagella. J Cell Biol 151, 709–718.

Pazour GJ, Dickert BL, Witman GB (1999). The DHC1b (DHC2) isoform of cytoplasmic dynein is required for flagellar assembly. J Cell Biol 144, 473–481.

Pazour GJ, Wilkerson CG, Witman GB (1998). A dynein light chain is essential for the retrograde particle movement of intraflagellar transport (IFT). J Cell Biol 141, 979–992.

Pazour GJ, Witman GB (2003). The vertebrate primary cilium is a sensory organelle. Curr Opin Cell Biol 15, 105–110.

Piperno G, Mead K, Henderson S (1996). Inner dynein arms but not outer dynein arms require the activity of kinesin homologue protein KHP1^{FLA10} to reach the distal part of the flagella in *Chlamydomonas*. J Cell Biol 133, 371–379.

Porter ME, Bower R, Knott JA, Byrd P, Dentler W (1999). Cytoplasmic dynein heavy chain 1b is required for flagellar assembly in *Chlamydomonas*. Mol Biol Cell 10, 693–712.

Rosenbaum JL, Witman GB (2002). Intraflagellar transport. Nat Rev Mol Cell Biol 3, 813–825.

Russell L, Ettlin R, Sinha Hikim A, Clegg E (1990). Histopathology of the testis. In: Histological and Histopathological Evaluation of the Testis, Clearwater, FL: Cache River Press, 210–266.

Sakai Y, Koyama Y, Fujimoto H, Nakamoto T, Yamashina S (1986). Immunocytochemical study on fibrous sheath formation in mouse spermiogenesis using a monoclonal antibody. Anat Rec 215, 119–126.

Sambrook J, Fritsch EF, Maniatis T (1987). Molecular Cloning, Cold Spring Harbor, NY: Cold Spring Harbor Laboratory Press.

San Agustin JT, Wilkerson CG, Witman GB (2000). The unique catalytic subunit of sperm cAMP-dependent protein kinase is the product of an alternative Calpha mRNA expressed specifically in spermatogenic cells. Mol Biol Cell 11, 3031–3044.

San Agustin JT, Witman GB (2001). Differential expression of the C_s and Cα1 isoforms of the catalytic subunit of cyclic 3',5'-adenosine monophosphate-dependent protein kinase in testicular cells. Biol Reprod 65, 151–164.

Sarpal R, Todi SV, Sivan-Loukianova E, Shirolikar S, Subramanian N, Raff EC, Erickson JW, Ray K, Eberl DF (2003). *Drosophila* KAP interacts with the kinesin II motor subunit KLP64D to assemble chordotonal sensory cilia, but not sperm tails. Curr Biol 13, 1687–1696.

Scholey JM (1996). Kinesin-II, a membrane traffic motor in axons, axonemes, and spindles. J Cell Biol 133, 1–4.

Scholey JM (2003). Intraflagellar transport. Annu Rev Cell Dev Biol 19, 423–443.

Signor D, Wedaman KP, Rose LS, Scholey JM (1999). Two heterotrimeric kinesin complexes in chemosensory neurons and sensory cilia of *Caenorhabditis elegans*. Mol Biol Cell 10, 345–360.

Sprando RL (1990). Perfusion of the rat testis through the heart using heparin. In: Histological and Histopathological Evaluation of the Testis, ed. LD Russel, RA Ettlin, AP Sinha Hikim, and ED Clegg, Clearwater, FL: Cache River Press, 277–280.

Taulman PD, Haycraft CJ, Balkovetz DF, Yoder BK (2001). Polaris, a protein involved in left-right axis patterning, localizes to basal bodies and cilia. Mol Biol Cell 12, 589–599.

Tokuyasu KT, Peacock WJ, Hardy RW (1972). Dynamics of spermiogenesis in *Drosophila melanogaster*. I. Individualization process. Z Zellforsch Mikrosk Anat 124, 479–506.

Tran PV, Haycraft CJ, Besschetnova TY, Turbe-Doan A, Stottmann RW, Herron BJ, Chesebro AL, Qiu H, Scherz PJ, Shah JV, *et al*. (2008). THM1 negatively modulates mouse sonic hedgehog signal transduction and affects retrograde intraflagellar transport in cilia. Nat Genet 40, 403–410.

Tsujikawa M, Malicki J (2004). Intraflagellar transport genes are essential for differentiation and survival of vertebrate sensory neurons. Neuron 42, 703–716.

van Dam TJ, Townsend MJ, Turk M, Schlessinger A, Sali A, Field MC, Huynen MA (2013). Evolution of modular intraflagellar transport from a coatomer-like progenitor. Proc Natl Acad Sci USA 110, 6943–6948.

Wicks SR, De Vries CJ, van Luenen HGAM, Plasterk RHA (2000). CHE-3, a cytosolic dynein heavy chain, is required for sensory cilia structure and function in *Caenorhabditis elegans*. Dev Biol 221, 295–307.

Witman GB (2003). Cell motility: deaf *Drosophila* keep the beat. Curr Biol 13, R796-R798.

Witman GB (2012). Dynein and intraflagellar transport. In: Dyneins: Structure, Biology and Disease, ed. SM King, New York: Elsevier, 395–421.

Wren KN, Craft JM, Tritschler D, Schauer A, Patel DK, Smith EF, Porter ME, Kner P, Lechtreck KF (2013). A differential cargo-loading model of ciliary length regulation by IFT. Curr Biol 23, 2463–2471.

Yamazaki H, Nakata T, Okada Y, Hirokawa N (1995). KIF3A/B: a heterodimeric kinesin superfamily protein that works as a microtubule plus end-directed motor for membrane organelle transport. J Cell Biol 130, 1387–1399.